Alma Mater Studiorum · Università di Bologna

Scuola di Scienze
Dipartimento di Fisica e Astronomia
Corso di Laurea in Fisica

Length Scale Calibration for van der Meer scans at the LHCb experiment

Relatore:
Dott. Fabio Ferrari

Correlatore:
Prof. Angelo Carbone

Presentata da:
Simone Di Giacinti

Anno Accademico 2023/2024

Abstract

The van der Meer scan is one of the main methods used in high-energy physics experiments to calibrate the luminosity. This method is based on moving the particle beams in precise positions to determine the beam profiles and thus the absolute luminosity scale. To verify that these beam movements are indeed accurate, each van der Meer scan (vdM) comprises a particular procedure called length scale calibration (LSC).
The following thesis presents the analysis of the data from three length scale calibration procedures, conducted at the LHCb experiment. The purpose of these procedures is to check the consistency between the nominal beam displacements (Δx_{LHC}, Δy_{LHC}), with the effective beam displacements (Δx_{VELO}, Δy_{VELO}). The compatibility of the two positions can be verified by checking if the quantities C_x and C_y, defined as the ratio between the measured and nominal beam displacement, minus one, are compatible with zero. To measure the effective displacements two different techniques were used: the constant beam separation method and the beam-gas imaging method.
The results obtained with the constant beam separation method are as follows:

- LSC 2022: $C_x = -0.0141 \pm 0.0005$; $C_y = -0.0057 \pm 0.0007$;
- First LSC 2023: $C_x = -0.0396 \pm 0.0015$; $C_y = -0.0407 \pm 0.0019$;
- Second LSC 2023: $C_x = -0.0442 \pm 0.0015$; $C_y = -0.0395 \pm 0.0019$.

The results obtained with the beam-gas imaging method are as follows:

- LSC 2022:
  - Beam 1: $C_x = -0.010 \pm 0.024$; $C_y = -0.020 \pm 0.029$;
  - Beam 2: $C_x = -0.002 \pm 0.032$; $C_y = 0.013 \pm 0.044$;
- First LSC 2023:
  - Beam 1: $C_x = 0.004 \pm 0.034$; $C_y = 0.003 \pm 0.027$;
  - Beam 2: $C_x = -0.003 \pm 0.033$; $C_y = -0.004 \pm 0.033$;
- Second LSC 2023:
  - Beam 1: $C_x = -0.013 \pm 0.032$; $C_y = -0.014 \pm 0.027$;
  - Beam 2: $C_x = 0.001 \pm 0.031$; $C_y = 0.002 \pm 0.034$.

These measurements will be complemented by a comprehensive evaluation of systematic uncertainties and will serve as input for the LHCb vdM campaign.

Abstract

La scansione di van der Meer è uno dei metodi principali utilizzati negli esperimenti di fisica delle alte energie per calibrare la luminosità. Questo metodo si basa sul movimento dei fasci di particelle in posizioni precise per determinare i profili dei fasci e quindi la scala della luminosità assoluta. Per verificare che questi movimenti dei fasci siano effettivamente accurati, ogni scansione di van der Meer (vdM) include una procedura particolare chiamata calibrazione della scala di lunghezza (LSC).
La seguente tesi presenta l'analisi dei dati presi da tre procedure di calibrazione della scala di lunghezza condotte nell'ambito dell'esperimento LHCb. Lo scopo di queste procedure è di controllare la compatibilità tra gli spostamenti nominali dei fasci (Δx_{LHC}, Δy_{LHC}), e i loro spostamenti effettivi (Δx_{VELO}, Δy_{VELO}). La compatibilità delle due posizioni può essere verificata controllando se le quantità C_x e C_y, definite come il rapporto tra lo spostamento nominale e misurato dei fasci, meno uno, sono compatibili con zero. Per misurare gli spostamenti effettivi sono state usate due tecniche differenti: il metodo della separazione costante dei fasci e il metodo dell'imaging fascio-gas.
I risultati ottenuti con il metodo della separazione costante dei fasci sono i seguenti:

- LSC 2022: $C_x = -0.0141 \pm 0.0005$; $C_y = -0.0057 \pm 0.0007$;
- Primo LSC 2023: $C_x = -0.0396 \pm 0.0015$; $C_y = -0.0407 \pm 0.0019$;
- Secondo LSC 2023: $C_x = -0.0442 \pm 0.0015$; $C_y = -0.0395 \pm 0.0019$.

I risultati ottenuti con il metodo dell'imaging fascio-gas sono i seguenti:

- LSC 2022:
  - Fascio 1: $C_x = -0.010 \pm 0.024$; $C_y = -0.020 \pm 0.029$;
  - Fascio 2: $C_x = -0.002 \pm 0.032$; $C_y = 0.013 \pm 0.044$;
- Primo LSC 2023:
  - Fascio 1: $C_x = 0.004 \pm 0.034$; $C_y = 0.003 \pm 0.027$;
  - Fascio 2: $C_x = -0.003 \pm 0.033$; $C_y = -0.004 \pm 0.033$;
- Secondo LSC 2023:
  - Fascio 1: $C_x = -0.013 \pm 0.032$; $C_y = -0.014 \pm 0.027$;
  - Fascio 2: $C_x = 0.001 \pm 0.031$; $C_y = 0.002 \pm 0.034$.

Queste misure saranno integrate da una valutazione completa delle incertezze sistematiche e verranno utilizzate come input per la campagna vdM dell'LHCb.

Contents

Introduction

The van der Meer scan is one of the principal techniques employed for calibrating luminosity at the Large Hadron Collider (LHC). This technique involves the precise displacement of the particle beams within the LHC ring. The accuracy of these beam displacements is critical for the success of the van der Meer scans, as they directly impact the precision of the luminosity measurements. To ensure that the displacements are performed with the required precision, each van der Meer scan includes a crucial step known as length scale calibration. This procedure allows the beam displacements to be precisely measured and it represents a key ingredient to achieve an accurate luminosity calibration.
This thesis is structured as follows. The first chapter begins with a brief introduction to the concept of luminosity in physics, followed by a presentation of the van der Meer scan and its mathematical foundations, with particular emphasis on the length scale calibration procedure. The second chapter provides an overview of the LHCb experiment, including a description of the various components of the LHCb detector.
The third chapter presents the analysis of the datasets corresponding to three length scale calibration campaigns that were performed during 2022 and 2023. It begins with an introduction to the data sample used, followed by a detailed explanation of the steps taken to implement two different measurement methods. Finally, the results are presented and discussed.

Chapter 1

The van der Meer scan method

The van der Meer scan method (vdM) is one of the primary methods for calibrating luminosity at the Large Hadron Collider (LHC) [1]. This method is named after the Dutch physicist Simon van der Meer, who invented it in 1968.
This chapter provides a brief introduction to the concept of luminosity in physics and a description of the vdM, with particular focus on a procedure, named length scale calibration (LSC), needed to achieve the ultimate precision in luminosity measurements at the LHC.

1.1 Luminosity in physics

In particle physics experiments the quantity that measures the ability of a particle accelerator to produce the required number of interactions is called luminosity and it represents the proportionality factor between the number of visible interactions per second ($\frac{d\mu}{dt}$) and the cross-section (σ) of a given process:

$$\mathcal{L} \cdot \sigma = \frac{d\mu}{dt}. \tag{1.1}$$

The previous formula is valid for fixed target experiments [2]. In case of colliding bunched beams, such as at the LHC, the luminosity formula takes a more complex form [4]:

$$\mathcal{L} = \nu_{riv} \cdot N_1 \cdot N_2 \cdot \Omega, \tag{1.2}$$

where ν_{riv} is the bunches revolution frequency, $N_{1,2}$ are the number of particles in the bunches 1 and 2, respectively, and Ω is the overlap integral of the 2 bunches with spatial density distributions $\rho_1(x, y, z, t)$ and $\rho_2(x, y, z, t)$. The overlap integral can be expressed as follows:

$$\Omega = K \cdot \iiiint \rho_1(x, y, z, t)\rho_2(x, y, z, t)\, dxdydzdt, \tag{1.3}$$

with $K = \sqrt{(\vec{v_1} - \vec{v_2})^2 - \frac{(\vec{v_1} \times \vec{v_2})^2}{c^2}}$ known as the kinematic factor, which can be approximated as $2c$ in the ultra-relativistic limit. Thus, the luminosity calibration involves the evaluation of the overlap integral, and one of the primary methods used at the LHC to estimate its value is known as van der Meer scan.

1.2 van der Meer scan

The key principle of the vdM scan method is to express the overlap integral in terms of rates that are experimental observables, rather than measuring the bunch density functions directly. Experimentally, the method consists in moving the beams across each other in two orthogonal directions. The overlap integral can be inferred from the rates measured at different beam separation values, provided the beam displacements are calibrated as absolute distances [4].
To illustrate the concept, let us consider the collision of two bunches moving in opposite directions with a number of particles equal to N_1 and N_2, respectively. If the first bunch is separated by $-\Delta x$, $-\Delta y$ from the second bunch in the plane perpendicular to the beams, the average number of interactions μ with cross section σ normalized by the number of particles is [1]:

$$\frac{\mu(\Delta x, \Delta y)}{N_1 \cdot N_2} = \sigma \cdot \frac{L}{N_1 \cdot N_2} = \sigma \cdot \iint \rho_1(x_2 + \Delta x, y_2 + \Delta y)\rho_2(x_2, y_2)\, dx_2 dy_2, \tag{1.4}$$

where L is the integrated luminosity and $\rho_{1,2}(x_2, y_2)$ are the normalized transverse particle densities of the unseparated bunches when $\Delta x = \Delta y = 0$. Integration over Δx and Δy drastically simplifies equation (1.4) since:

$$\iiiint \rho_1(x_2 + \Delta x, y_2 + \Delta y)\rho_2(x_2, y_2)\, dx_2 dy_2 d\Delta x d\Delta y = 1, \tag{1.5}$$

as can be easily proved by substituting $x_1 = x_2 + \Delta x$ e $y_1 = y_2 + \Delta y$. In the new variables the integrals $\iint \rho_1(x_1, y_1)\, dx_1 dy_1$ and $\iint \rho_2(x_2, y_2)\, dx_2 dy_2$ decouple and reduce to unity by definition. From equations (1.4), (1.5) one can obtain the van der Meer formula:

$$\sigma = \iint \frac{\mu(\Delta x, \Delta y)}{N_1 \cdot N_2}\, d\Delta x d\Delta y, \tag{1.6}$$

where $\mu_{sp} \equiv \frac{\mu(\Delta x, \Delta y)}{N_1 \cdot N_2}$ is often referred to as the specific number of interactions. The attribute "specific" underlines that different physics processes and detectors would inevitably produce and detect a different number of interactions, respectively. Equation (1.6) can be interpreted as follows: from the perspective of the second bunch, the first bunch is moving, and those transverse movements smear and "wash out" its profile ρ_1, effectively making it constant $\overline{\rho_1}$. This reduces the complicated overlap integral, assuming

ρ_1 and ρ_2 are normalized, to:

$$\iint \overline{\rho_1}\rho_2 \, dx_2 dy_2 = 1. \tag{1.7}$$

The same reasoning can be applied from the frame of reference of first bunch, leading to the same result. It is important to note that in practice, the beams do not move continuously, but are displaced stepwise, since it would be impossible to synchronize exactly all the magnets to achieve continuous movement.
In accelerators, it is also impossible to guide all particles perfectly parallel to the ideal trajectory. Therefore, in any accelerator the optical elements are designed to return particles that deviate from the ideal trajectory, causing them to oscillate in the transverse plane. To ensure stable operation, the accelerator is designed such that the oscillatory motions are separately stable in the transverse coordinates x and y and are almost independent of each other (x-y factorization). These motions also shape the density profiles ρ_1 and ρ_2, so, assuming the x-y factorization holds, the densities can be also factorized as follows:

$$\rho_{1,2}(x, y) = \rho^x_{1,2}(x) \cdot \rho^y_{1,2}(y). \tag{1.8}$$

Furthermore, from equation (1.4), the factorization of μ_{sp} follows directly, reducing the integral in equation (1.6) to two one-dimensional integrals along the lines $\Delta x = \Delta x_0$ e $\Delta y = \Delta y_0$:

$$\begin{aligned}
\sigma &= \iint \mu_{sp}(\Delta x, \Delta y) \, d\Delta x \, d\Delta y \\
&= \int \mu^x_{sp}(\Delta x) \, d\Delta x \int \mu^y_{sp}(\Delta y) \, d\Delta y \frac{\mu^y_{sp}(\Delta y_0)\mu^x_{sp}(\Delta x_0)}{\mu^y_{sp}(\Delta y_0)\mu^x_{sp}(\Delta x_0)} \\
&= \frac{\int \mu_{sp}(\Delta x, \Delta y_0) \, d\Delta x \times \int \mu_{sp}(\Delta x_0, \Delta y) \, d\Delta y}{\mu_{sp}(\Delta x_0, \Delta y_0)}.
\end{aligned} \tag{1.9}$$

The above formula is valid for every point $(\Delta x_0, \Delta y_0)$, and the integrals in the enumerator can be measured in two one-dimensional scans over Δx (or Δy), with Δy_0 (or Δx_0) fixed. It might be advantageous to choose $(\Delta x_0, \Delta y_0)$ not far from the point of maximal luminosity to collect sufficient statistics of interactions.
At the LHC, x-y factorization is generally good, but not perfect. Any imperfection in the accelerator, that leads to an x–y coupling, disrupts this factorization. The cross-section corrections due to x–y non-factorizability and the associated systematic errors are typically at the level 1%.

1.3 Length Scale Calibration

From equation (1.6), it follows that the measurement of the cross section is directly affected by any errors on the displacements Δx e Δy of the beams. An accurate measurement of the Δx, Δy scale is performed in a dedicated length scale calibration procedure, which always accompanies van der Meer scans [1]. Let's assume that the true beam positions $\vec{\Delta}_i$ in the laboratory frame for the beam i = 1, 2 can be written as:

$$\vec{\Delta}_i = \alpha_i \vec{a}_i + \beta_i \vec{b}_i + \vec{\Delta}_i^0, \tag{1.10}$$

where α_i and β_i are the, exactly known, nominally set values for x-y movements and $\vec{a_i}$, $\vec{b_i}$ are unknown vectors close to, but not exactly equal, the unit x, y-vectors. The constant vectors $\vec{\Delta}_i^0$ are the initial positions, which are also unknown.
In the simplest LSC the beams are nominally displaced by the same amount, so $\alpha_1 = \alpha_2 = \alpha_{LSC}$ and $\beta_1 = \beta_2 = \beta_{LSC}$. If the bunches have equal shapes, the center of the luminous region ($\vec{O}_{LSC}$) is positioned midway between them:

$$\vec{O}_{LSC} = \alpha_{LSC} \frac{\vec{a}_1 + \vec{a}_2}{2} + \beta_{LSC} \frac{\vec{b}_1 + \vec{b}_2}{2} + \frac{\vec{\Delta}_1^0 + \vec{\Delta}_2^0}{2}. \tag{1.11}$$

This position can be accurately measured by a vertex locator.
Most often van der Meer scans are performed moving the beams symmetrically in opposite directions, to reach maximal separations within the limited range of beam movements. This means that $\alpha_1 = -\alpha_2 = 2\alpha_{sym}$ and $\beta_1 = -\beta_2 = 2\beta_{sym}$, so the difference between the beam positions can be expressed as follows:

$$\vec{\Delta}_{1,2} = \vec{\Delta}_1 - \vec{\Delta}_2 = \alpha_{sym} \frac{\vec{a}_1 + \vec{a}_2}{2} + \beta_{sym} \frac{\vec{b}_1 + \vec{b}_2}{2} + \frac{\vec{\Delta}_1^0 - \vec{\Delta}_2^0}{2}. \tag{1.12}$$

Combining equations (1.11), (1.12) it shows that from a measurement of $\vec{O}_{LSC}$, the scales $\frac{\vec{a}_1+\vec{a}_2}{2}$, $\frac{\vec{b}_1+\vec{b}_2}{2}$ necessary for a symmetric scan can be derived.
In the case of non-symmetric scans, the relative position of the beams depends on linear combinations of $\frac{\vec{a}_1+\vec{a}_2}{2}$ and $\frac{\vec{b}_1+\vec{b}_2}{2}$, which can also be derived through a measurement of $\vec{O}_{LSC}$. Alternatively the simplest way to individually calibrate the lengths $|\vec{a}_{1,2}| = a_{1,2}$ and $|\vec{b}_{1,2}| = b_{1,2}$ is using luminosity measurements. Ideally the luminosity should remain constant during an LSC, so any small variation indicates a change in the distance between the beams. For example, consider the LSC in the x direction. Assuming that the factorization x-y holds and neglecting the angle between $\vec{a}_{1,2}$ and the x-axis, one arrives at the scalar equations:

$$\Delta_{i,x} = \alpha_{LSC} a_i + \Delta_{0,i,x}, \tag{1.13}$$

$$\Delta_{12,x} = \alpha_{LSC}(a_1 - a_2) + (\Delta_{1,x}^0 - \Delta_{2,x}^0), \tag{1.14}$$

$$O_{LSC,x} = \alpha_{LSC} \frac{a_1 + a_2}{2} + \frac{\Delta_{1,x}^0 + \Delta_{2,x}^0}{2}. \tag{1.15}$$

The difference between the luminous region positions, at two distinct points of the LSC, allows to find the average of the x scale:

$$\frac{a_1 + a_2}{2} = \frac{O^1_{LSC,x} - O^2_{LSC,x}}{\alpha^1_{LSC} - \alpha^2_{LSC}}. \tag{1.16}$$

The corresponding change in the x distance between the beams, $\Delta^1_{12,x} - \Delta^2_{12,x}$, can be deduced from the luminosity change $L^1_{LSC} - L^2_{LSC}$ and van der Meer scan data. Considering a symmetric vdM along the x direction, the beam separation change required to modify the luminosity by a given amount can be calculated from the derivative ($\frac{d\Delta_{12,x}}{dL} = \frac{d\alpha_{sym}}{dL} \cdot \frac{a_1+a_2}{2}$). This leads to the equation:

$$\Delta^1_{12,x} - \Delta^2_{12,x} = (\alpha^1_{LSC} - \alpha^2_{LSC})(a_1 - a_2) = \frac{d\alpha_{sym}}{dL} \cdot \frac{a_1 + a_2}{2}(L^1_{LSC} - L^2_{LSC}), \tag{1.17}$$

which allows to obtain $\frac{a_1-a_2}{a_1+a_2}$ from the measurable values of $\frac{d\alpha_{sym}}{dL}$, $L^1_{LSC} - L^2_{LSC}$ and $\alpha^1_{LSC} - \alpha^2_{LSC}$. This knowledge, along with the value of $\frac{a_1+a_2}{2}$ from equation (1.16), permits the individual calibration of the scales $a_{1,2}$.
To improve the sensitivity of the method and increase $L^1_{LSC} - L^2_{LSC}$, LSC can be performed at a point close to the maximum of the derivative $\frac{dL}{d\Delta_{12,x}}$, where the second derivative is zero. For Gaussian bunches with the widths $\sigma_{1,2}$, the luminosity dependence on the beam separation is also Gaussian with the sigma $\Sigma = \sqrt{\sigma_1^2 + \sigma_2^2}$, and the optimal LSC beam separation is $\Delta_{12} = \Sigma$.

Chapter 2

The LHCb experiment

The LHCb detector is one of the four main experiments at the Large Hadron Collider (LHC) at CERN in Geneva. This chapter begins with a brief introduction to the LHC, followed by a more detailed discussion of the LHCb detector, with particular focus on the Vertex Locator and SMOG systems, which have played a fundamental role in the analysis presented in Chapter 3.

2.1 Large Hadron Collider

The Large Hadron Collider is the world's largest particle accelerator, located beneath the CERN complex, spreading across the French-Swiss border, at varying depths from 45 m to 170 m [7]. The LHC was constructed using the pre-existing ring, which is 26.7 km long and was originally built between 1984 and 1989 for the Large Electron-Positron Collider (LEP). The LHC primarily accelerates beams of protons, divided into bunches of approximately 10^{11} particles each. These beams move in opposite directions and collide at designated points, in which are located the detectors of four experiments. Currently, during active operation periods, two bunches collide every 25 ns generating an energy of 13.6 TeV in the centre-of-mass frame of reference. Figure 2.1 provides a pictorial representation of the LHC ring, within the CERN accelerator complex.

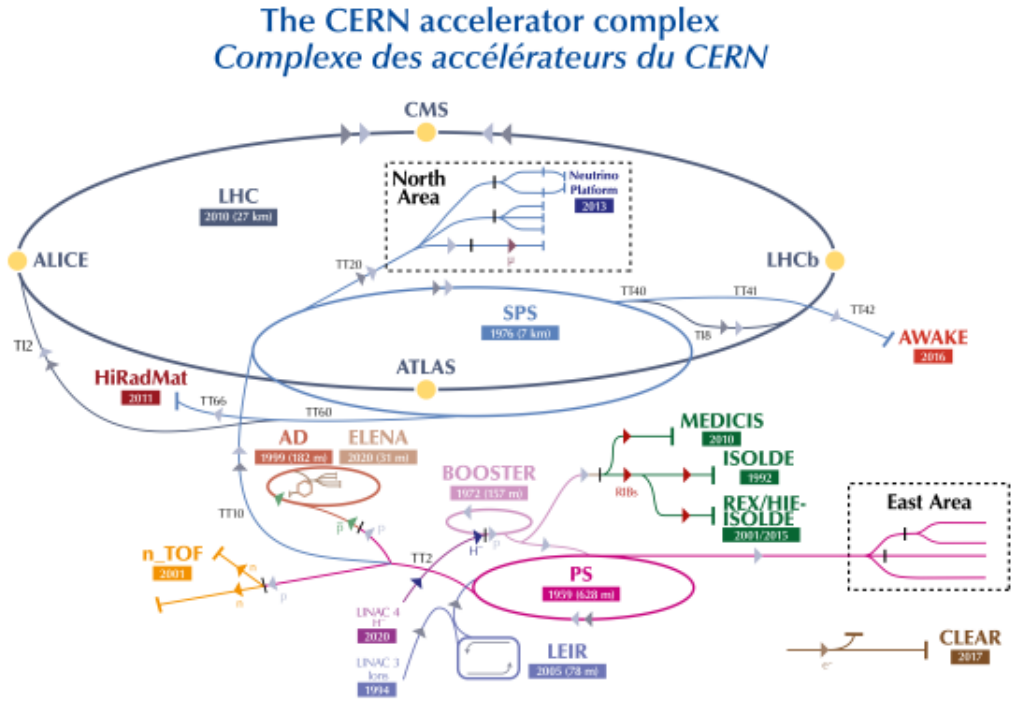

Figure 2.1: Scheme of the CERN accelerator [6].

2.2 The LHCb detector

The LHCb experiment is one of the four large detectors at the Large Hadron Collider accelerator at CERN. Its main purpose is the research of new physics through studies of CP violation and rare decays of heavy-flavour hadrons [3]. The experiment was originally designed to collect data at a maximum instantaneous luminosity of $\mathcal{L} = 2 \times 10^{32} cm^{-2} s^{-1}$, but it was successfully operated for most of Run 1 (2010-2012) and Run 2 (2015-2018) at $\mathcal{L} \sim 4 \times 10^{32} cm^{-2} s^{-1}$. At the end of Run 2, nearly all the LHCb sub-detectors were almost completely renewed in order to operate the experiment at a nominal instantaneous luminosity $\mathcal{L} = 2 \times 10^{33} cm^{-2} s^{-1}$ and to collect events at the LHC crossing rate of 40 MHz, from the beginning of Run 3. To this end, the trigger strategy was also updated. Starting from Run 3, events are discriminated by an all-software trigger that reconstructs all events in real time at the visible interaction rate of approximately 30 MHz.

2.2.1 Detector layout

The LHCb detector is a single-arm forward spectrometer located at interaction point number 8 (IP8) on the LHC ring [3]. The components of the LHCb detector can be di-

vided in two groups, based on their function. The first group comprises an array of pixel silicon detectors surrounding the interaction region, called the Vertex Locator (VELO), the silicon-strip Upstream Tracker (UT) in front of the large-aperture dipole magnet, and three Scintillating Fibre Tracker (SciFi Tracker) stations downstream of the magnet. The dipole magnet is used to measure the momenta of particles, using a vertical magnetic field [5]. These sub-detectors form the tracking particle system.
The second group handles particle identification, and consists of two ring imaging Cherenkov detectors (RICH1 and RICH2) using C_4F_{10} and CF_4 gases as radiators, a shashlik-type electromagnetic calorimeter (ECAL), an iron-scintillator tile sampling hadronic calorimeter (HCAL), and four stations of muon chambers (M2-5) interleaved with iron shielding. Figure 2.2 shows a lateral view of the upgraded detector layout.

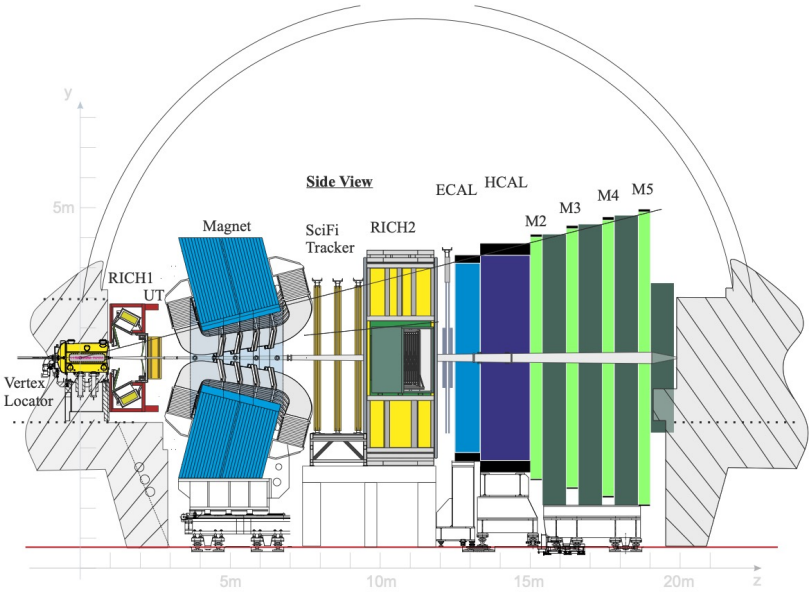

Figure 2.2: Layout of the upgraded LHCb detector

2.2.2 Vertex locator

The Vertex Locator (VELO) detects tracks of ionising particles coming from the beam collision region, thereby measuring the location of interaction vertices, displaced decay vertices and the distances between them. The core technology of the VELO is pixelated hybrid silicon detectors, which are arranged into identical modules. These modules are positioned perpendicular to the beam line, covering the full pseudorapidity acceptance of

LHCb ($2 < \eta\ ^1 < 5$) and ensuring that most tracks from the interaction region traverse at least four pixel sensors, for all azimuthal directions. To satisfy these requirements, 52 modules are necessary. Moreover the modules are divided in two identical halves, except for a shift along z-axis[2] : Side A and Side C. Figure 2.3 shows two perspectives of the modules arrangement.

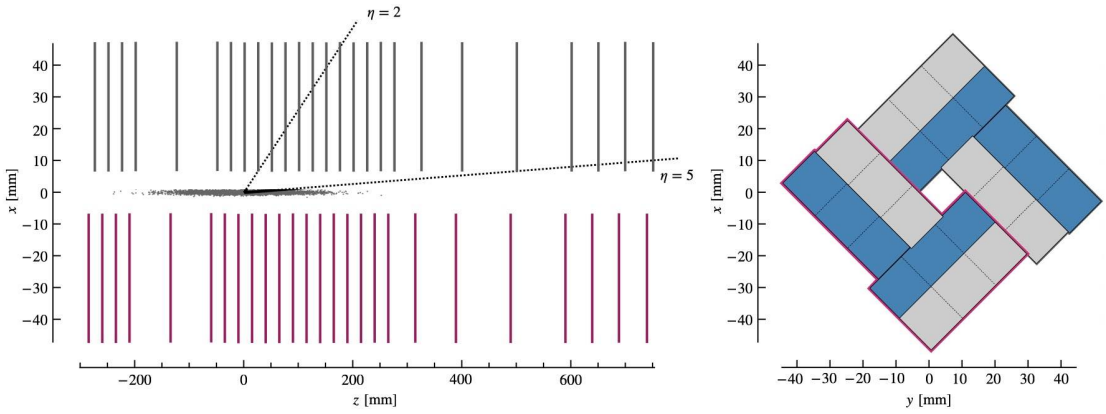

Figure 2.3: Left: schematic top view of the z-x plane at y = 0 (left) with an illustration of the z-extent of the luminous region and the nominal LHCb pseudorapidity acceptance, $2 < \eta < 5$. Right: sketch showing the nominal layout of the rectangular pixel detectors around the z-axis in the closed VELO configuration. Half the detectors are placed on the upstream module face (grey) and half on the downstream face (blue). The modules on the Side C are highlighted in purple on both sketches [3].

To be compatible with improved experimental conditions, some components of the VELO were completely renewed. In particular, the RF boxes, which enclose the detector and interface it with the LHC beams, were entirely redesigned reducing both the material and the inner radius of the VELO along the beam line. Furthermore, a new structure, a storage cell, is fitted immediately upstream of the VELO detector in the beam vacuum. This cell performs a fundamental role in the SMOG system, which is described in Section 2.3. The combination of the pixel geometry, a smaller distance to the first measured point and reduced material means the performance of the VELO is significantly improved, compared to Run 1 and Run 2. However, the closer proximity to the LHC collisions and the increase in design luminosity means the detector will have to cope with hit rates and radiation doses that are an order of magnitude higher than those experienced by the

[1] $\eta \equiv -ln(tan\frac{\theta}{2})$ where θ is the angle between the particle momentum $\vec{p}$ and the positive direction of the beam axis.

[2] The coordinate system used has the origin at the nominal pp interaction point, the z axis along the beam pointing towards the muon system, the y axis pointing vertically upward and the x axis defining a right-handed system.

previous VELO [3].
As mentioned previously in Section 1.3, the precise position measurements provided by a vertex locator are fundamental for the LSC. Therefore, the VELO played a crucial role in the analysis presented in Chapter 3, furnishing the data used.

2.2.3 Magnet

The dipole magnet consists of two identical, saddle-shaped coils, which are mounted symmetrically inside a window-frame yoke. Each coil is made from five triplets of aluminium pancakes and is supported by cast aluminium clamps fixed to the yoke. The magnet provides a vertical magnetic field with a bending power of $\simeq 4$ Tm and, during data taking periods, its polarity is reversed regularly (every few weeks) to collect data sets of roughly equal size with the two field configurations. Through this magnetic field, the magnet contributes to the measurement of charged particles momenta.

2.2.4 Trackers

The tracking particle system contains two trackers: the Upstream Tracker (UT) and the Scintillating Fibre Tracker (SciFi Tracker).
The UT is located between the RICH1 detector and the dipole magnet. It is used for charged-particle tracking and provides an initial determination of the track momentum p with moderate precision ($\sim 15\%$) [3]. The UT detector comprises four planes of silicon detectors organised in two stations. Each station consists in a vertical plane and an inclined plane by $+5°$ and $-5°$ respectively, as shown in Figure 2.4.

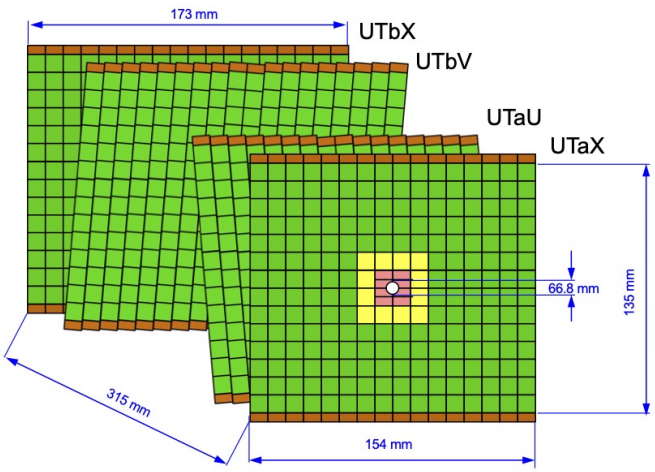

Figure 2.4: Drawing of the four UT silicon planes with indicative dimensions. Different colours designate different types of sensors: Type-A (green), Type-B (yellow), Type-C and Type-D (pink) [3].

The SciFi Tracker is located downstream of the LHCb dipole magnet, and, like the UT, it is responsible for charged particle tracking and momentum measurement. The SciFi Tracker uses a single detector technology based on plastic scintillating fibres arranged in multilayered fibre mats. In total there are 12 detection planes arranged in 3 stations (T1, T2, T3) with 4 layers each in an X-U-V-X configuration, as shown in Figure 2.5. The X layers have their fibres oriented vertically and are used for determining the deflection of the charged particle tracks caused by the magnetic field. The U and V layers have their fibres rotated by $\pm 5^{\circ}$ in the plane of the layer for reconstructing the vertical position of the track hit.

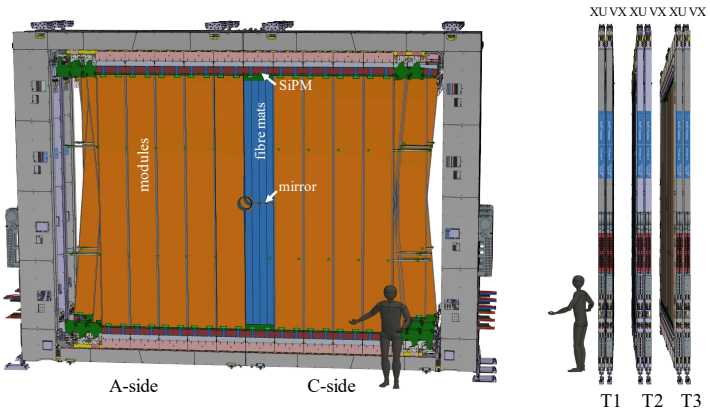

Figure 2.5: Front and side views of the 3D model of the SciFi Tracker detector.

2.2.5 RICH detectors

The RICH system consists of two detectors: RICH1 and RICH2 (Figure 2.6). RICH1 and RICH2 cover angular acceptances from 25 to 300 mrad and from 15 to 120 mrad in the magnet bending plane, respectively; and from 25 to 250 mrad and 15 to 100 mrad in the vertical direction. The system provides hadron particle identification (PID) in the momentum range of 2.6 to 100 GeV/c^2 [3]. Specifically RICH1, located upstream of the magnet, employs a C_4F_{10} gas radiator, allowing it to provide PID in the momentum range of 2.6 to 60 GeV/c^2. RICH2 is located downstream of the magnet and it handles PID for particles with higher momentum, between 15 and 100 GeV/c^2, using a CF_4 gas radiator. Both RICH1 and RICH2 have photon detector planes: in RICH1, they are located above and below the detector, while in RICH2, they are at the sides of the detector. To read out the detectors at a 40 MHz rate, the entire photon detection chain was replaced in both RICH1 and RICH2, since the system, used during Run 1 and Run 2, was limited to a 1 MHz output rate.

Figure 2.6: Schematic view of the (left) RICH1 and (right) RICH2 detectors [3].

2.2.6 Calorimeters

The LHCb calorimeter system presents a classical structure of an electromagnetic calorimeter (ECAL) followed by a hadronic calorimeter (HCAL). The ECAL is laterally segmented in three regions, with increasing dimensions going from the beam pipe outwards, in order to cope with different hit densities across its surface. The regions are segmented in square cells that scale with the distance from the beam-pipe, as shown in Figure 2.7 (left), to maintain a roughly uniform particle rate per cell. The ECAL cells have a shashlik structure, consisting of alternated scintillator and lead layers.
The HCAL is a sampling tile calorimeter, with a structure made up of staggered iron and plastic scintillator tiles mounted parallel to the beam axis to enhance the light collection. Like the ECAL, the HCAL is divided in two regions, which are further segmented in square cells (Figure 2.7, right). However, it has a larger granularity than the ECAL, given the typical spread of hadronic showers.
The two calorimeters share the same basic detection principle: scintillation light from plastic scintillator modules is transmitted to the photomultiplier tubes (PMTs) by wavelength-shifting fibres. Fibre bundles from calorimeter modules are then fed to the PMTs. In order to have a constant energy scale across the calorimeter surface, the gain of the ECAL and HCAL PMTs is set proportionally to the distance from the beam pipe of the corresponding modules.

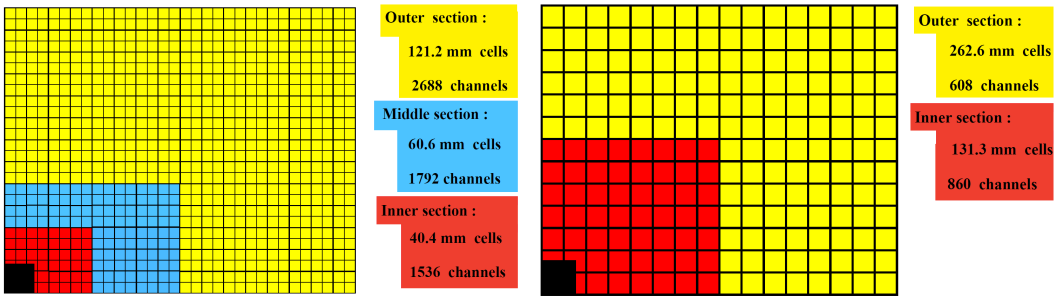

Figure 2.7: Lateral segmentation of (left) the ECAL and (right) the HCAL. One quarter of the detector front face is shown [3].

2.2.7 Muon detector

The LHCb muon detector is composed of four stations M2 to M5, located downstream of the calorimeter system. During the Run 1 and Run 2 the muon system additionally included a station M1 located upstream of the calorimeters, which was utilised in the old hardware trigger and it is no longer needed in the upgraded system.
Each station is composed of two halves and divided into four regions, R1 to R4, of increasing area moving from the central beam axis outwards. The area and the segmentation of the four regions scale in such a way to uniformly distribute the particle flux and the channel occupancy across each station. The four stations are equipped with multi-wire proportional chambers (MWPCs), which are made up of four independent layers, each consisting of anode wires between two cathode planes [3].

2.3 System for Measuring Overlap with Gas

The system for measuring overlap with gas (SMOG) was originally designed to inject light noble gas into the VELO vacuum vessel, enabling precise colliding-beams luminosity calibration. This injection created a temporary local pressure increase peaking at around 10^{-7} mbar over the length of the vessel and decaying down to the LHC background level ($\sim 10^{-9}$ mbar) over the 20 m LHCb beam pipe sections on each side of the interaction point [3].
The modern upgraded SMOG (also known as SMOG2) consists mainly of two systems: the storage cell assembly, mounted inside the beam vacuum, and the gas feed system (GFS), located on the "balcony", a platform near the detector inside the experimental cavern. The storage cell comprises two cylindrical halves, each attached to the upstream end of one of the VELO detector halves, moving together with them, as shown in Figure 2.8. When the VELO is in the closed position, the two halves form an open-ended tube coaxial with the LHC beam axis. The GFS is responsible for the injection of gas at a

controlled flux, via a capillary at the centre of the storage cell, creating a triangular gas density distribution that peaks at the injection point.
The SMOG upgrade introduced many improvements, starting from an increased areal density at an identical injected flux. Furthermore, the determination of the target density (and beam-gas luminosity) is significantly more precise because the target is confined to the storage cell, also leading to a much better defined beam-gas collision region, well separated from the beam-beam collision region.

For all the features listed above, SMOG has played an important role in the analysis presented in Chapter 3, improving the study of beam-gas (beam-empty) and gas-beam (empty-beam) data in the length scale calibration process.

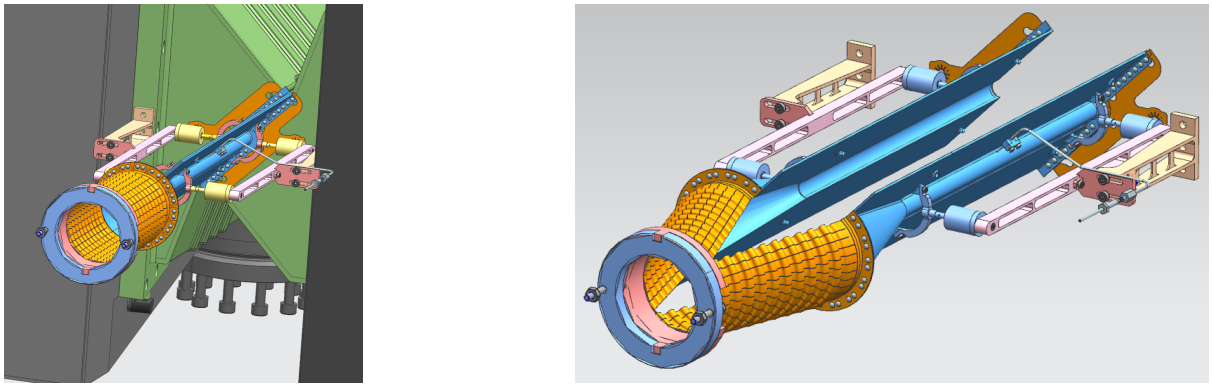

Figure 2.8: Left: view of the storage cell (blue) supported from the VELO RF box flanges (in green) in the closed VELO position. Right: storage cell in the open position (without showing VELO elements) [3].

Chapter 3

Measurement of the length scale calibration constants

In this chapter, two methods for obtaining the absolute length scale calibration are presented. These methods are discussed following a description of the analysed data sample.

3.1 Data Sample

The data sample used in this analysis was collected during two van der Meer scans. The first scan took place on 10th November 2022, starting at 07:22:14 and ending at 11:20:33. The other scan was conducted on 7th September 2023, from 15:41:51 to 21:15:44, and comprised two length scale calibration procedures. The data required for this analysis were obtained from a CERN database named NXCALS, using an interface called TIMBER, and from the LHCb dataset collected during the van der Meer (vdM) campaigns. For each vdM scan studied, the collected data can be dived in two groups:

- The first group comprises the information provided by the LHC, such as the beam nominal positions (x and y), which were stored in a CSV file.
- The second group comprises the information obtained from the LHCb detector, which were stored in two ROOT files.

The CSV files contain data about the beam nominal positions (x and y), during the vdM, their associated timestamp, expressed in human-readable date (for example 7th September 2023 at 19:02:35) and an incremental number, known as vdM step, used to uniquely identify the different beam displacements.

The data used in this analysis, stored in the ROOT files, are the following:

- Interaction vertices positions (x,y and z), measured by the VELO. These events are selected by a random trigger to avoid any bias due to candidates selected by physics lines.
- The type of collision, or crossing, corresponding to a given vertex. There are four possible crossing types:
  - Beam-Beam (bb) Crossing: A collision occurs between a bunch from beam 1 and a bunch from beam 2.
  - Beam-Empty (be) Crossing: A collision occurs between a bunch from beam 1 and the gas in the beam pipe, but there is no bunch from beam 2.
  - Empty-Beam (eb) Crossing: The opposite of the previous one, so there is a collision between a bunch from beam 2 and the gas.
  - Empty-Empty (ee) Crossing: No bunches are present in either beam.

  In this analysis the first three types were studied.
- The number of complete revolutions that a bunch has made around the LHC ring, since the LHCb data acquisition started, later referred to as orbitNumber. This number is reset to zero each time a LHCb run is started. A LHCb run represents the time window in which the LHCb detector collects data and can have a maximum length of one hour.
- The number that identifies a specific bunch crossing, later referred to as bxId. The LHC ring has 3564 slots in which the bunches can be injected and a given bunch is identified by its injection slot. Therefore this number ranges from 0 to 3563. During van der Meer scans only a few bunches are injected.

The last two information were used to evaluate the correct detection time of the vertices. This can be easily done using the following formula:

$$time = t_0 + \frac{orbitNumber \cdot 3564 + bxId}{40.078 \times 10^6}, \tag{3.1}$$

where t_0 is the time, corresponding to the start of a given run, 3564 is the number of injection slots in the LHC ring and 40.078×10^6 is the crossing frequency of all the LHC bunches, corresponding to 11245 revolutions per second for each bunch.
The data from both groups were aligned using the epoch time (the details of this operation are explained in Section 3.2). Unix epoch time, or Unix time, refers to the number of seconds that have elapsed since 1st January 1970 (midnight UTC), excluding leap seconds.

Although the term “epoch” literally refers to Unix time 0, it is often used as a synonym for Unix time.
The analysis is centred on the length scale calibration procedure (LSC), therefore only some parts of the van der Meer scans were studied. Specifically in the 2022 vdM (Figure 3.1, up) the length scale calibration process started at 10:05:24 and ended at 10:41:19. In the 2023 vdM (Figure 3.1, down), the first and the second LSC were performed from 18:30:44 to 19:02:35 and from 19:05:40 to 19:37:30, respectively. In Figure 3.2 are graphically shown the beam movements during the length scale calibration procedures.

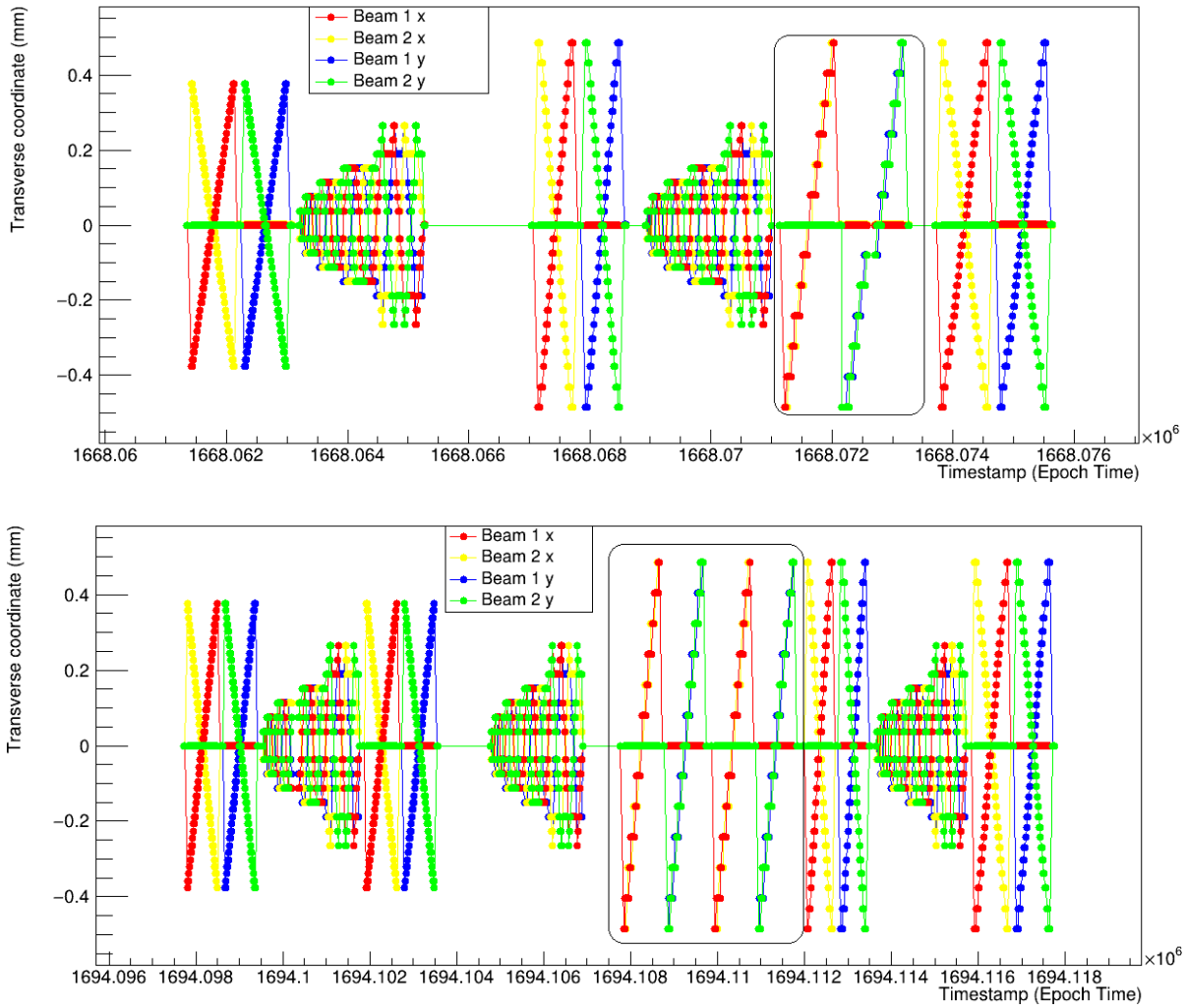

Figure 3.1: Beam movements during van der Meer scans performed in 2022 (up) and 2023 (down). The red and yellow lines represent the x coordinate of the first and second beam, respectively. Similarly, blue and green lines represent the y coordinate of the first and second beam, respectively. The LSC regions can be identified by looking for coincident movements of the x or y coordinates of both beams, and they have been highlighted with a black frame.

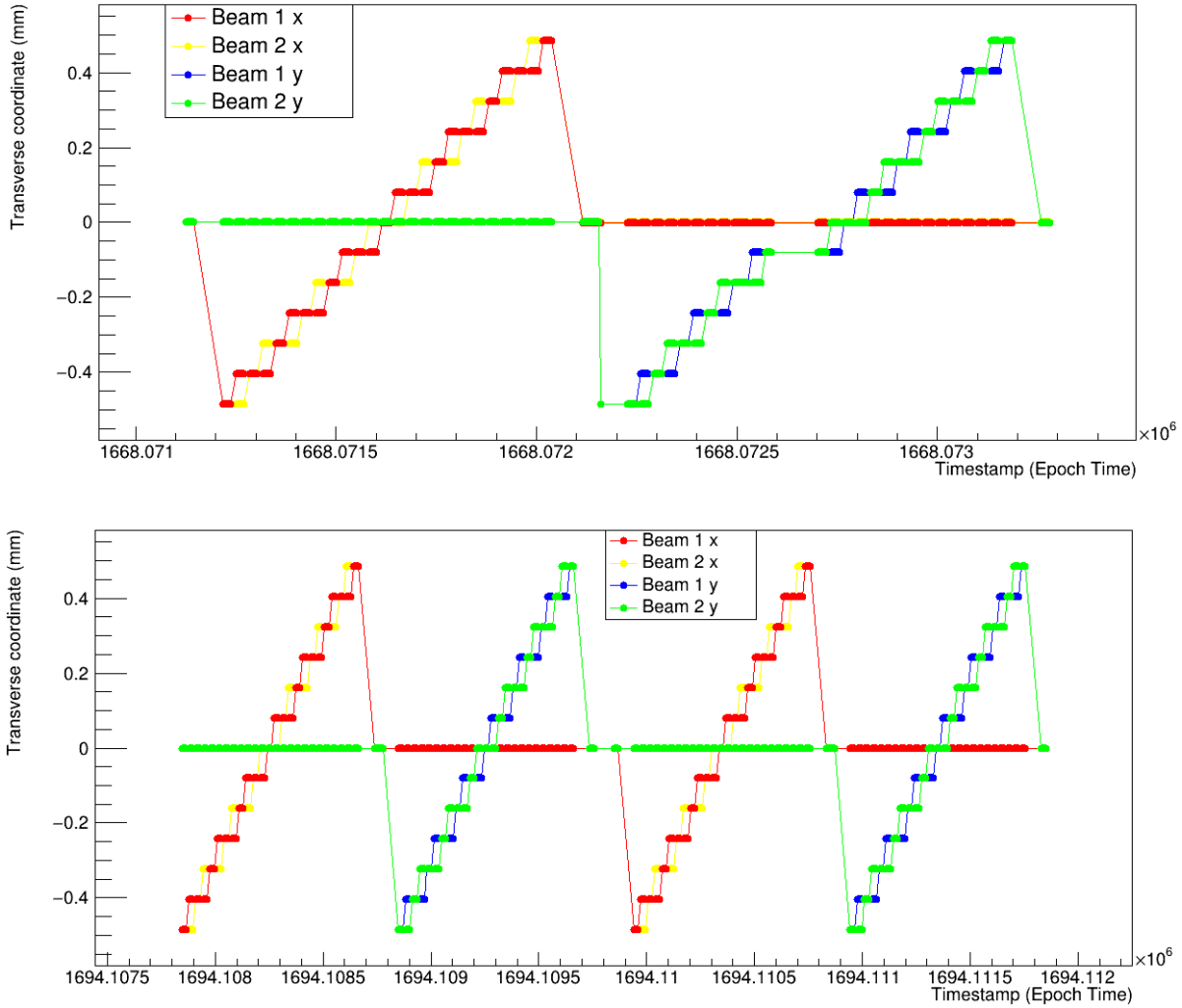

Figure 3.2: Up: beam nominal positions during the LSC performed in 2022 vdM. Down: beam nominal positions during the first and second LSC performed consecutively in 2023 vdM. The meaning of the different colors is explained in the caption of Figure 3.1. From the pictures are clearly visible the alternate one-dimensional movements of the beams coordinates.

3.2 Data Analysis

The goal of this analysis is to verify that the nominal displacement of the beams (Δx_{LHC}, Δy_{LHC}) aligns with the actual displacement (Δx_{VELO}, Δy_{VELO}), measured through the interaction vertices positions reconstructed by the VELO. The compatibility of the two positions can be verified by checking if the length scale calibration constants, defined as [4]:

$$C_x = \frac{\Delta x_{VELO}}{\Delta x_{LHC}} - 1, \tag{3.2}$$

$$C_y = \frac{\Delta y_{VELO}}{\Delta y_{LHC}} - 1, \tag{3.3}$$

are compatible with zero. The quantities defined above have been measured with two different techniques: the constant beam separation method and the beam-gas imaging method.
In order to measure these quantities, the datasets needed to be treated to ensure an efficient analysis. Using a Python script, in particular employing a library called Pandas, the following manipulations were performed on the CSV file of each scan:

- Conversion of the human-readable date in epoch time, and alignment with the ROOT files' epoch time, by subtracting 7200 seconds from the CSV timestamps. Of this, 3600 seconds accounted for the different time zones used in the CSV and ROOT files, while the other 3600 seconds accounted for the use of daylight saving time in the CSV file but not in the ROOT file.

- Identification of the time ranges corresponding to the length scale calibration steps, by looking for coincident movements of the x or y coordinates of both beams on the whole van der Meer scan plot.

After finding the time range for each LSC, another Python script was used on each CSV file, to determine the time limits for each time step in the length scale calibration procedure. Each LSC involved spatial displacement of each coordinate through 13 spatial steps, conducted over 26 time steps. As shown in Figure 3.2, the beams were moved one at a time from one spatial step to the next. Therefore, although there are only 13 spatial displacements (or spatial steps) for each coordinate, moving the beams through these 13 spatial steps required 26 time intervals (or time steps). Knowing the time steps it was possible to evaluate the beam nominal displacements Δx_{LHC}, Δy_{LHC} from the data stored in the CSV file.
For the 2022 vdM scan, incomplete data from the two ROOT files led to the analysis being limited to the first 12 spatial steps for the x coordinate movement and the last 8 spatial steps for the y coordinate movement. For the 2023 van der Meer scan, data from all steps was available and used.

3.2.1 Constant beam separation method

This method consists on moving the beams in equidistant spatial steps in Δx and Δy, keeping their nominal separation constant. During the translation of both beams, the centre of the luminous region should follow the beam positions. The luminous region centre can be determined using beam-beam vertices measured with the VELO.
In the length scale calibration procedures analysed, the beam nominal separation was zero, so the centre of the luminous region was coincident with the beam measured positions. As shown in Figure 3.2, there are time steps in which the beam nominal separation is not zero. For this method those intervals have been neglected because they didn't comply with the method's requirements.
The following operations were conducted for each LSC analysed. Using a C++ script, two histograms were created and filled for each valid time step. These histograms, shown in Figure 3.3, were populated with the x and y coordinates of the beam-beam crossing vertices. Only the vertices that fell within the time range corresponding to each specific time step were included in the related histograms. Furthermore, during the filling process, in order to remove background from material interactions[1], only vertices that lied within 3 mm from the origin of the axes were retained. Another C++ script was used to realize two two-dimensional graphs, one for each coordinate. In these graphs the mean of each histogram, which represent the beam measured position, was plotted against the corresponding time step, as shown in Figure 3.4.
Using another C++ script, an additional graph for each coordinate was created, where both the beam measured position and the corresponding beam nominal position (x or y) were plotted along the y-axis, against the time steps. To cope with the offset between the origin of the VELO frame of reference and the origin of the LHC frame of reference, two alignment methods were implemented:

- Sideband method: As shown in Figure 3.4, for each coordinate, the length scale calibration procedure comprises a part in which the coordinate is kept constant, later referred to as sideband. A C++ script was developed to compute the mean value of the sideband, and then shift the beam measured positions by that quantity. This resulted in the overlap of the sidebands of the beam measured positions graph and of the beam nominal positions graph, and consequently, the rest of both graphs as well.

[1]Material interactions refer to the physical interactions that occur between particles and the materials in a detector or experimental setup. These processes can produce signals or "background noise" that might interfere with the primary measurements being made in the experiment.

- Fit[2] method: A C++ script was used to find the global displacement that results in best data-LHC position compatibility. To do so, a chi squared (χ^2), defined as follows

$$\chi^2 = \sum_{step} \frac{(measured - nominal - p_0)^2}{err^2}, \tag{3.4}$$

was minimised, where the sum is extended on all the steps in which the given coordinate is not in the sideband position. "Measured" and "nominal" represent the beam measured and nominal position (x or y) in the given step, respectively. "Err" is the uncertainty on the beam measured position and, finally, p_0 is the unknown parameter to be found through the chi squared minimisation procedure. After finding p_0 the beam measured positions were shifted by that quantity, as in the previous method.

The graphical result of these two methods is shown in Figures 3.5 and 3.6, respectively. The alignment methods were also employed, in a further C++ script, to create another graph for each coordinate. In these graphs the difference between the beam nominal and measured positions was represented, after applying the alignment methods, against the corresponding beam nominal position. Clearly only the steps in which the given coordinate (x or y) was being moved are plotted. These graphs are showed in Figure 3.7 for both alignment methods.
Lastly, the mean value of the spatial displacement for each coordinate was computed from the beam measured positions. The results obtained through the constant beam separation method are discussed in Section 3.3.

[2]Fit: The process of adjusting a mathematical function (often derived from a theoretical model) to best describe experimental observations. This adjustment procedure involves finding the best estimators for the free parameters of the function, ensuring that the latter accurately reflects the observed data.

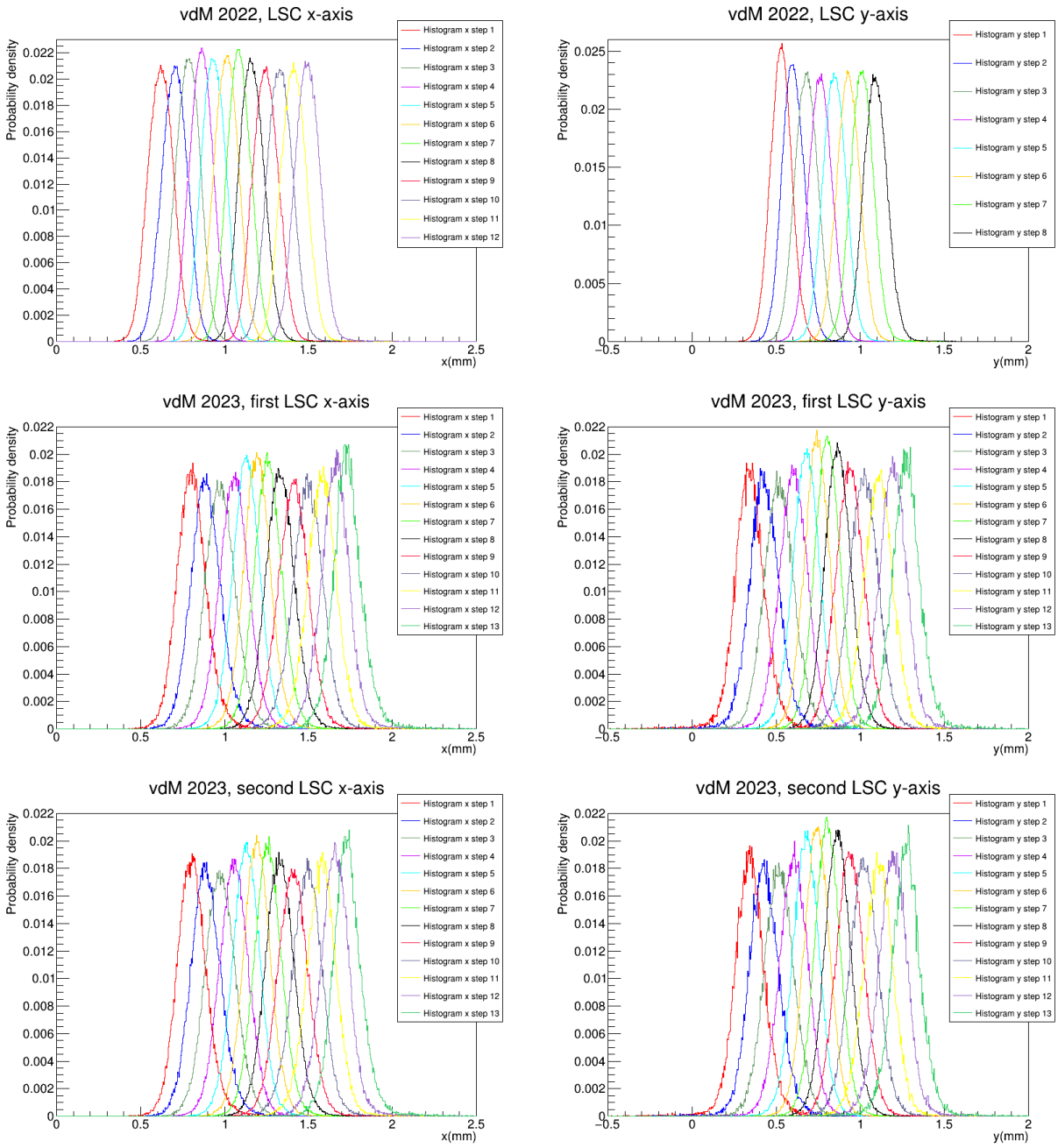

Figure 3.3: Beam-beam vertex distributions, through the spatial steps. Each plot displays more histograms, to show the beam movements. The histograms were normalised to unit area to allow for a better comparison.

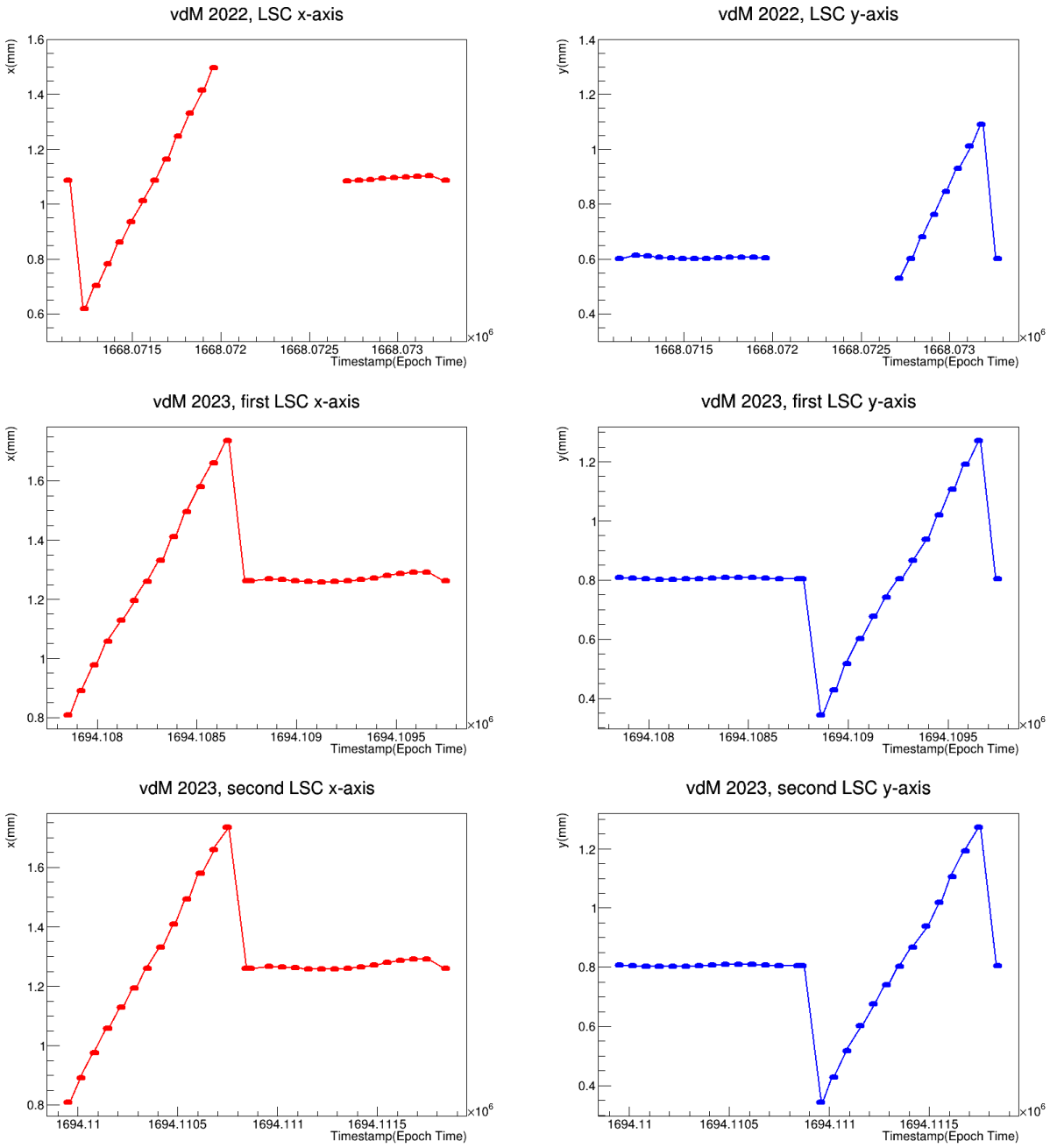

Figure 3.4: Beam measured positions plotted against the time steps. In the graphs showing the 2022 LSC is visible a central empty region, due to the lack of data, mentioned previously. The red markers and lines represent the movements of the x coordinate, the blue ones represent the movements of the y coordinate.

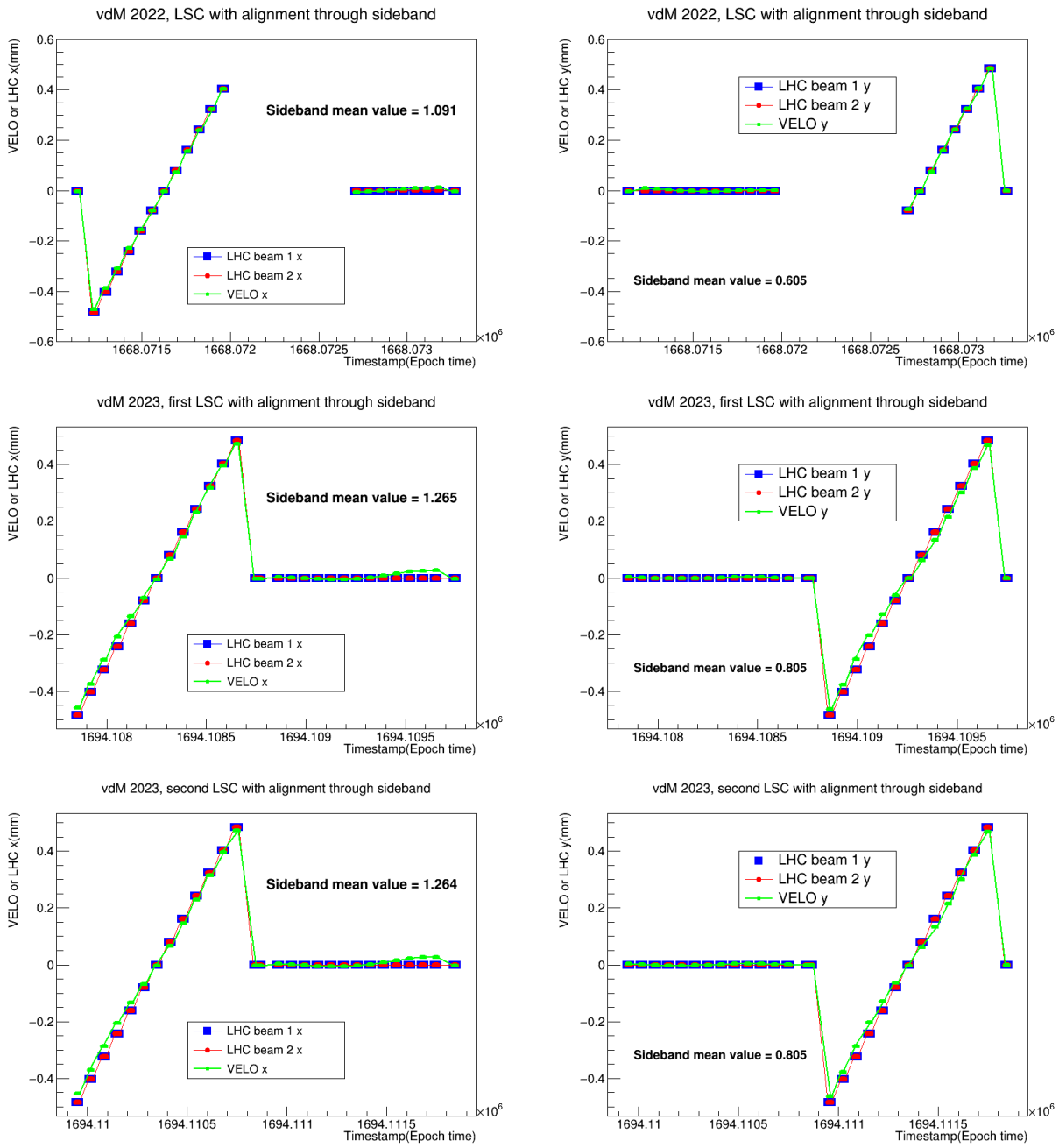

Figure 3.5: Beam measured and nominal positions, aligned using the "sideband method", plotted against the time steps. In the graphs showing the 2022 LSC is visible a central empty region, due to the lack of data, mentioned previously.

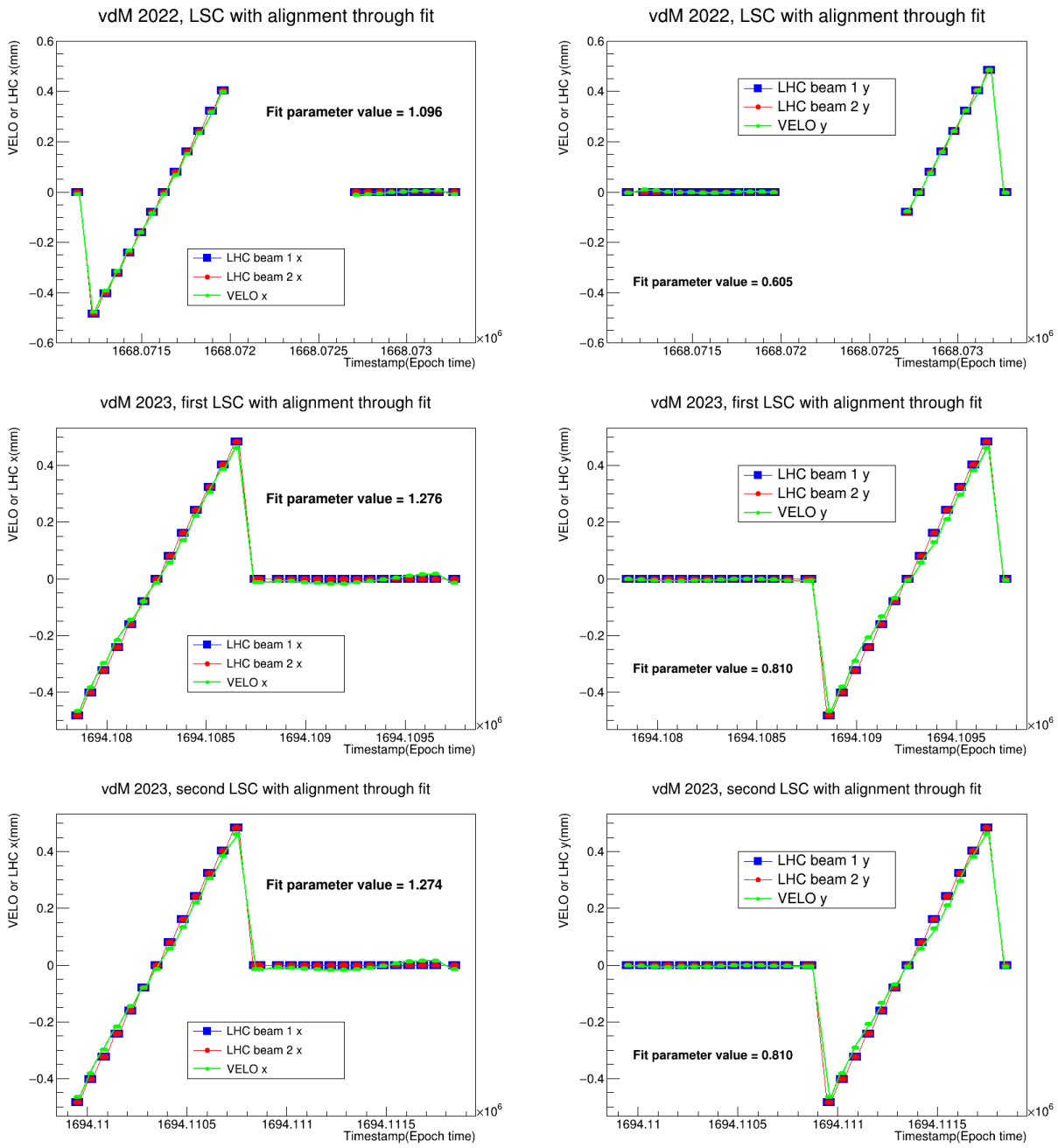

Figure 3.6: Beam measured and nominal positions, aligned using the "fit method", plotted against the time steps. In the graphs showing the 2022 LSC is visible a central empty region, due to the lack of data, mentioned previously.

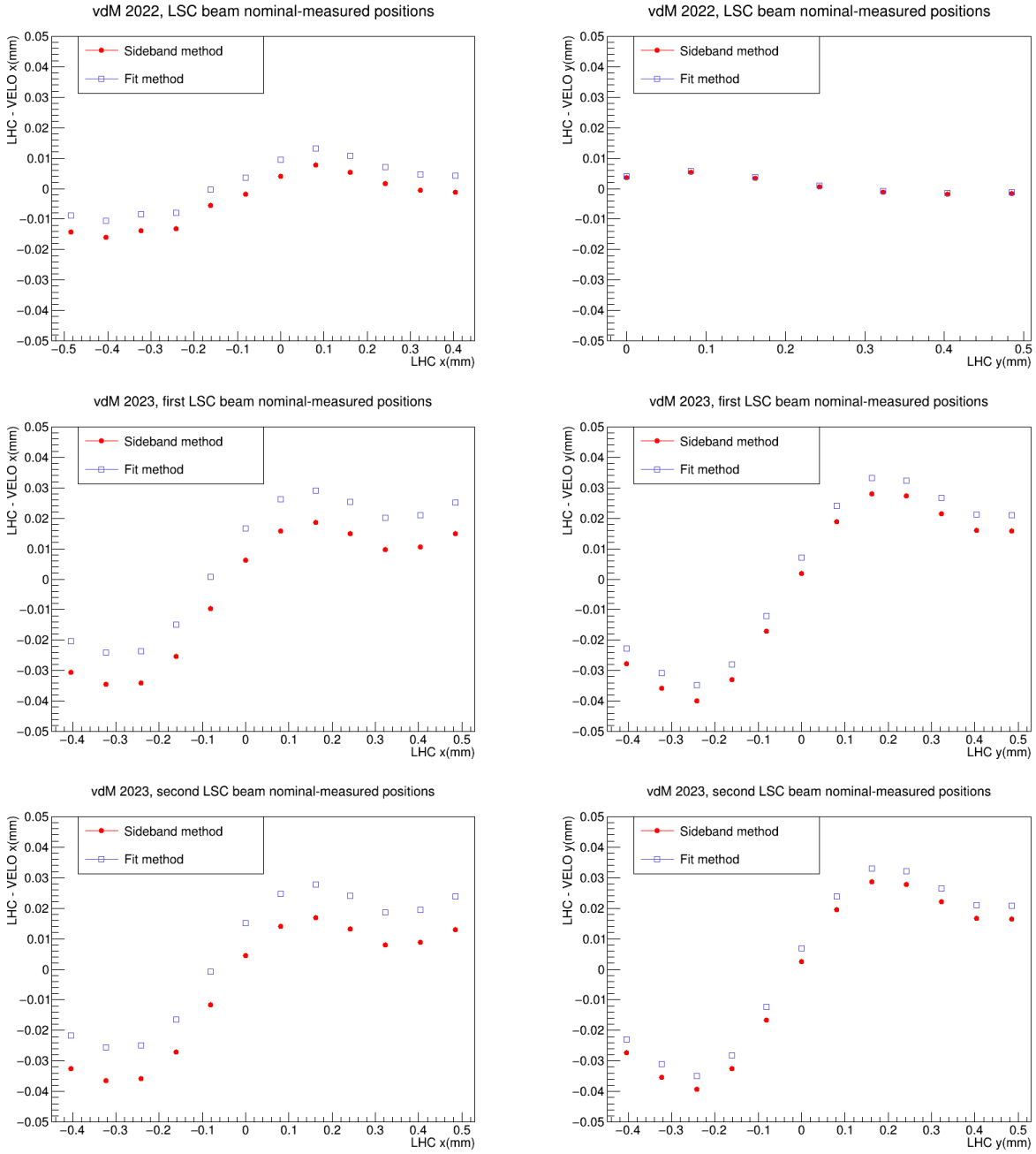

Figure 3.7: Difference of the beam nominal and measured positions, after applying the "sideband method"or the "fit method", plotted against the beam nominal position. The error bars are very small and therefore not visible, due to the large statistical sample of beam-beam vertices. In the graph depicting the 2022 LSC along the y-axis, there are fewer points compared to the others due to the previously mentioned data shortage.

3.2.2 Beam-gas imaging method

In the beam-gas imaging method the beam positions are measured individually, using beam-gas interaction vertices reconstructed by VELO. The beam-gas vertices include the beam-empty (be) and the empty-beam (eb) interaction vertices. As in the constant beam separation method, the beams are moved in equidistant spatial steps along the x-axis and y-axis. However, for this method, all the time steps were considered since there is no requirement for constant beam separation, unlike in the former method.
The operations carried out for each LSC analyzed to implement this method are similar to those in the previous method, with a few minor changes. These actions were conducted separately for beam-empty and empty-beam vertices:

- Creating and filling two histograms, one for each coordinate, for every time step. These histograms were filled with the x and y coordinate of the interaction vertices (be or eb), within the corresponding time step, respectively. Only the vertices that lied within 3 mm from the origin of the axes were retained, to remove background from material interactions. Figures 3.8 and 3.9 show the histograms filled with beam-empty vertices and empty-beam vertices, respectively.

- Creating two graphs, one for each coordinate, in which the beam measured position (the histogram mean) was plotted against the related time step. This is shown in Figure 3.10 for beam 1 (be vertices) and in Figure 3.11 for beam 2 (eb vertices).

- Realizing an additional graph for each coordinate, plotting the time steps on the x-axis and both the beam measured and nominal positions on the y-axis. The "sideband method" and the "fit method", described in Section 3.2.1, were applied to align the positions. These graphs are showed in Figures 3.12, 3.13, for beam 1 and in Figures 3.14, 3.15 for beam 2.

- Creating a graph for each coordinate, to show the difference between the beam nominal and measured positions, after the application of the alignment methods, against the beam nominal position. The result of this operation is shown in Figure 3.16. In these graphs the time steps in which the beams had the same nominal position are plotted.

- Computing the mean value of the beam measured displacements Δx_{VELO}, Δy_{VELO} for both beams, from their measured positions.

The results of the beam-gas imaging method are presented in Section 3.3.

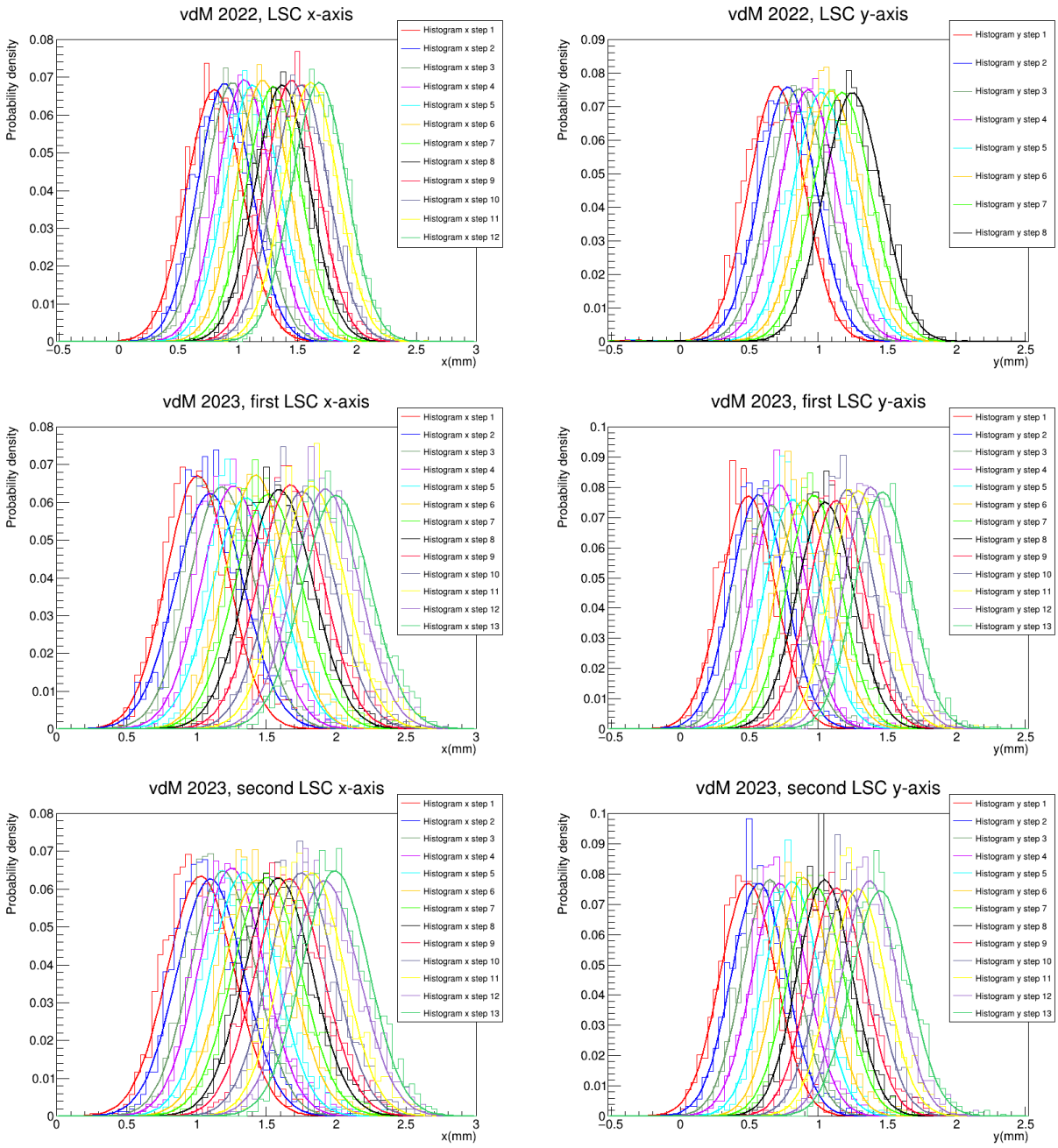

Figure 3.8: Beam-empty vertex distributions, through the spatial steps. Each plot comprises more histograms and each histogram is displayed with a Gaussian function fitted on the histogram itself. This function was necessary to improve the clarity of the plots, and to display more evidently the beam 1 movements. The histograms were normalised to unit area to allow for a better comparison.

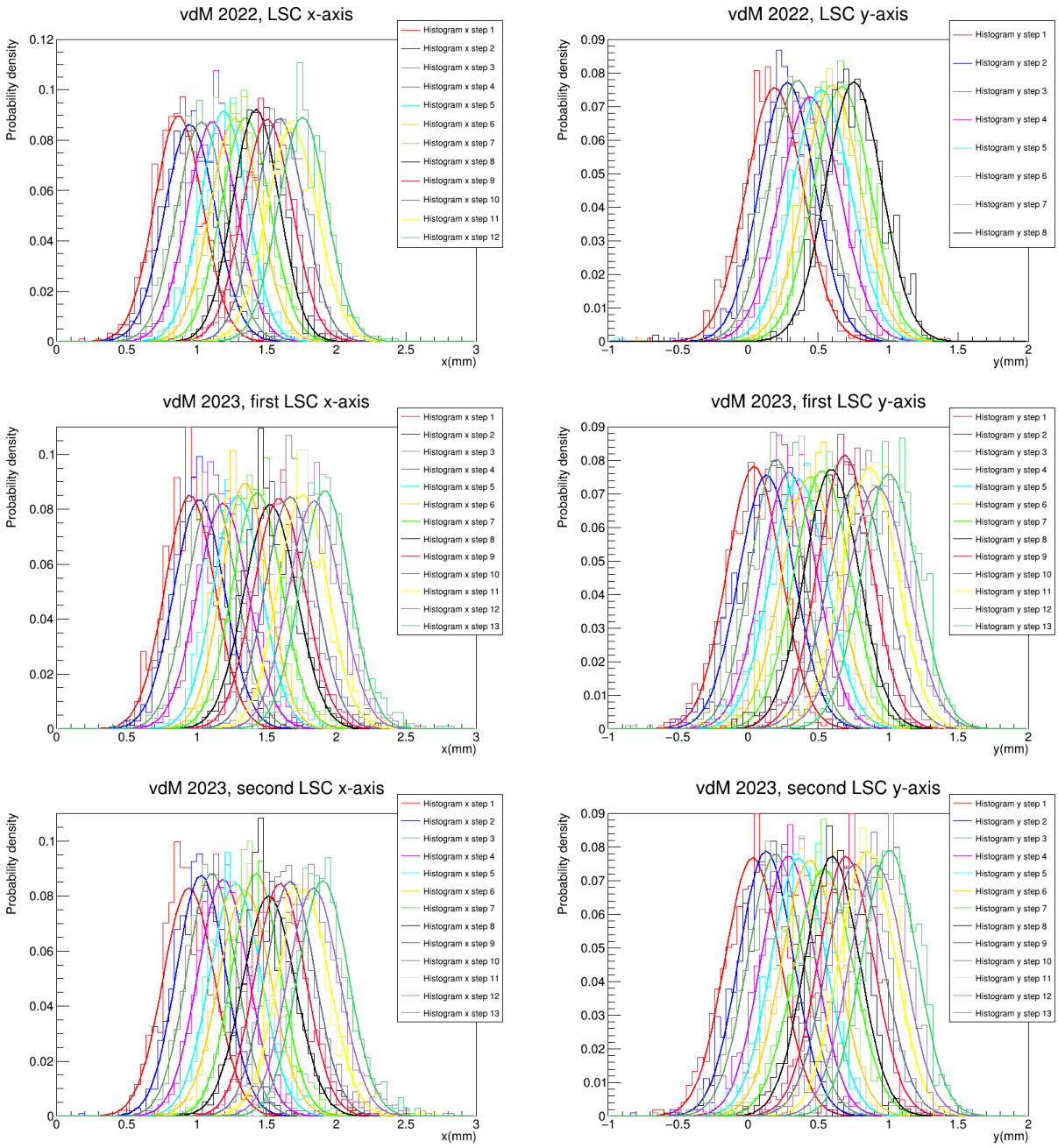

Figure 3.9: Empty-beam vertex distributions, through the spatial steps. Each plot comprises more histograms and each histogram is displayed with a Gaussian function fitted on the histogram itself. This function was necessary to improve the clarity of the plots, and to display more evidently the beam 2 movements. The histograms were normalised to unit area to allow for a better comparison.

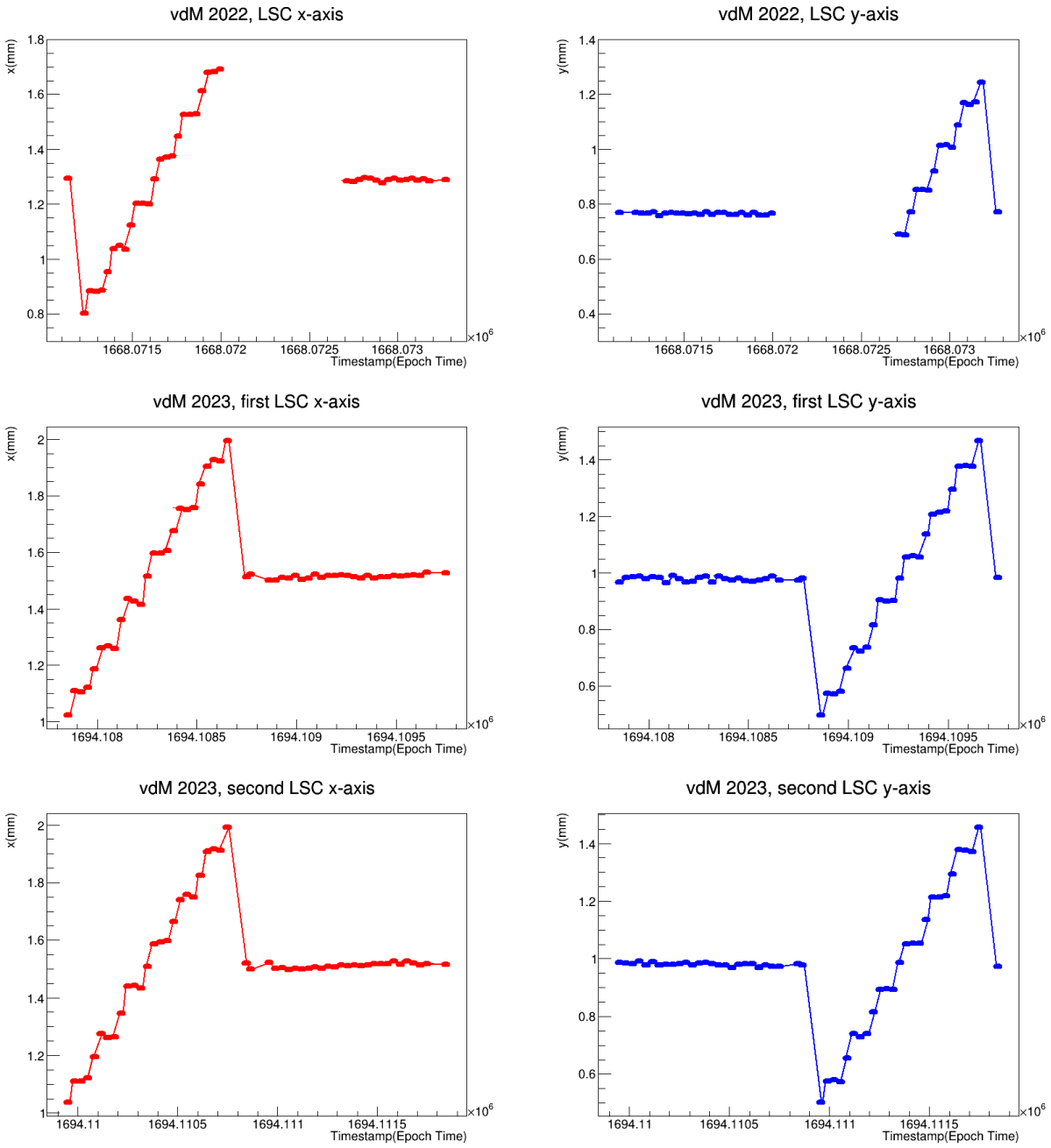

Figure 3.10: Beam 1 measured position plotted against the time steps. In the graphs showing the 2022 LSC is visible a central empty region, due to the lack of data, mentioned previously. The red markers and lines represent the movements of the x coordinate, the blue ones represent the movements of the y coordinate.

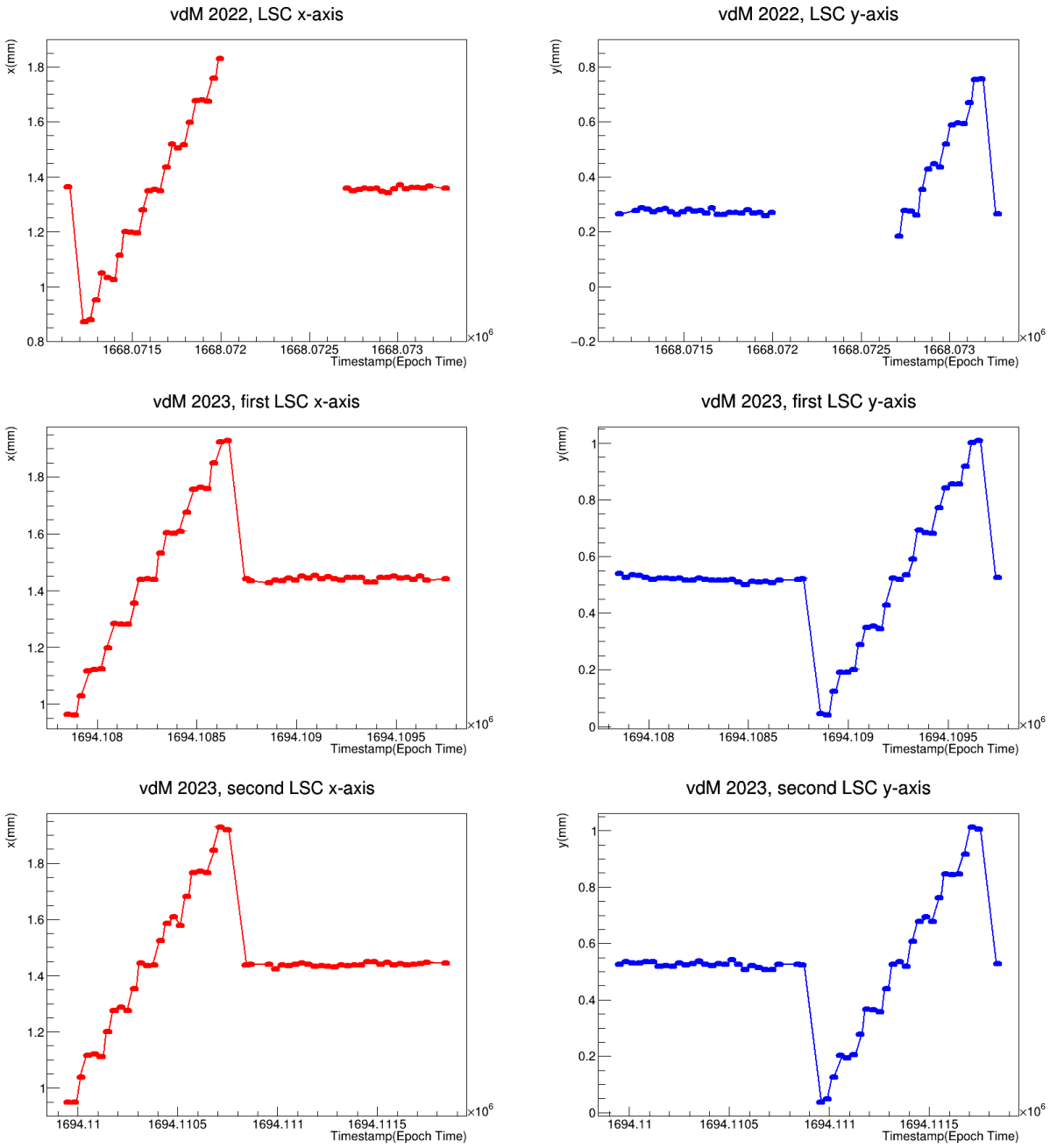

Figure 3.11: Beam 2 measured position plotted against the time steps. In the graphs showing the 2022 LSC is visible a central empty region, due to the lack of data, mentioned previously. The red markers and lines represent the movements of the x coordinate, the blue ones represent the movements of the y coordinate.

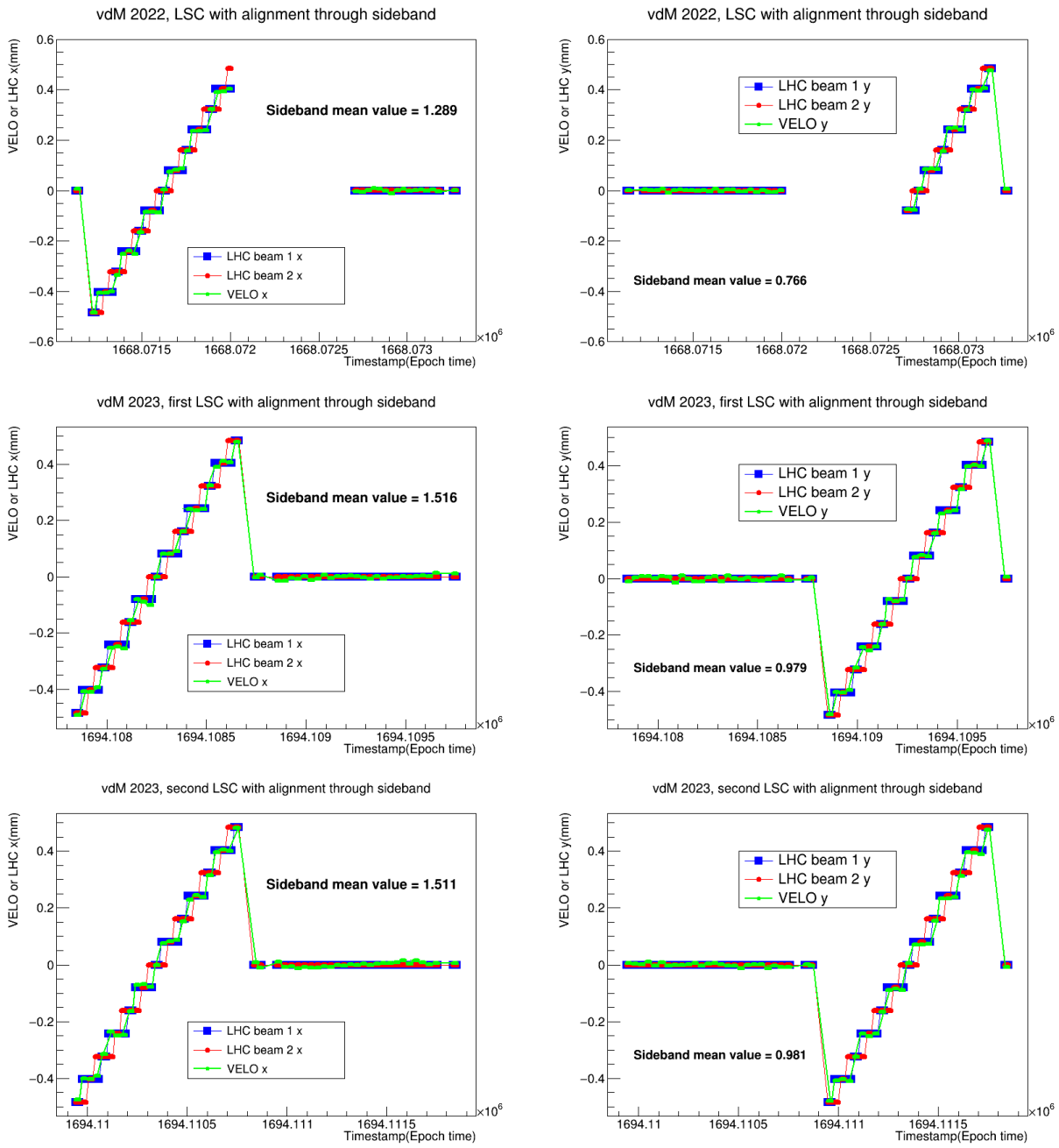

Figure 3.12: Beam 1 measured position and both beams nominal positions, aligned using the "sideband method", plotted against time steps. In the graphs showing the 2022 LSC is visible a central empty region, due to the lack of data, mentioned previously.

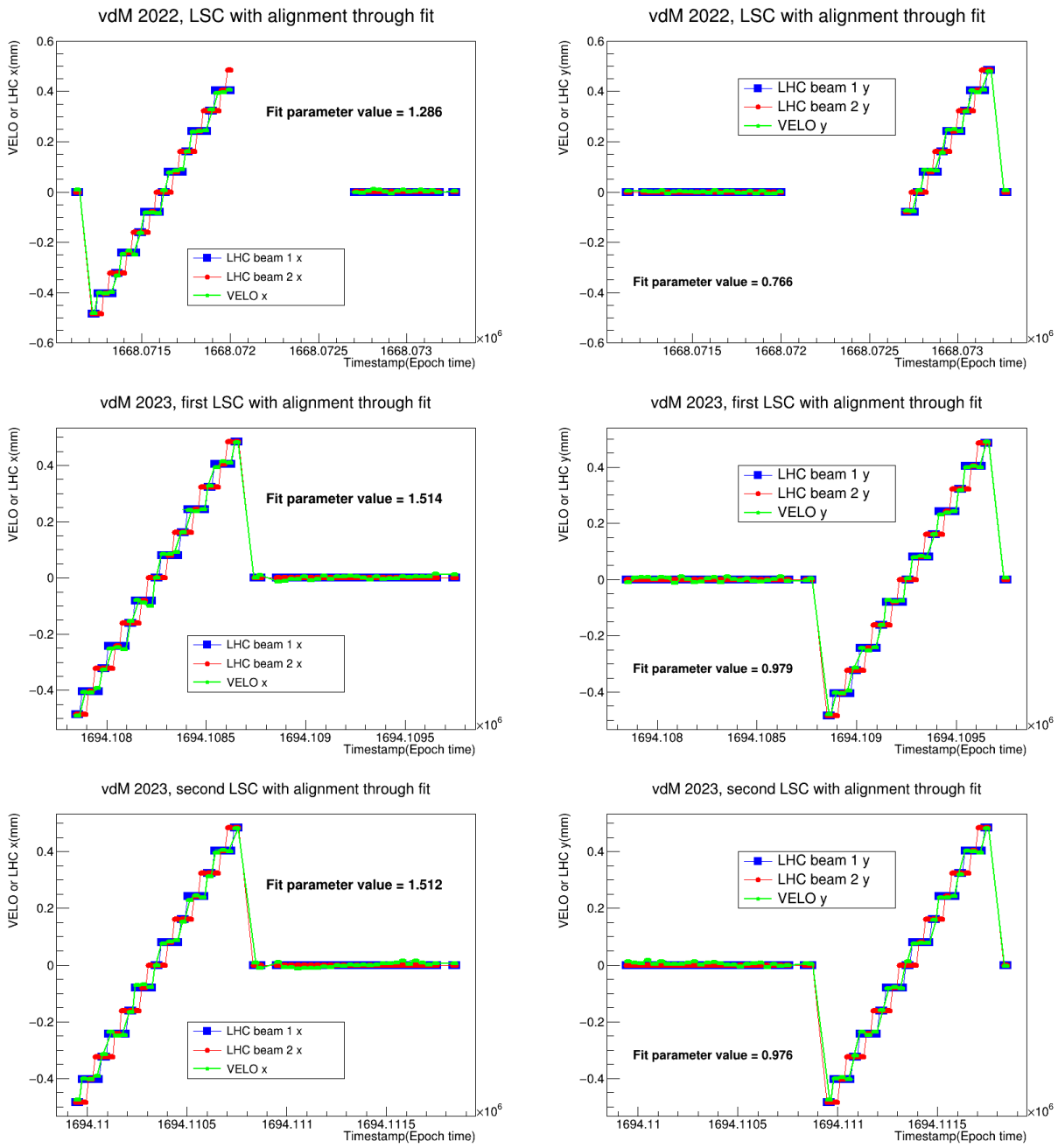

Figure 3.13: Beam 1 measured position and both beam nominal positions, aligned using the "fit method", plotted against time steps. In the graphs showing the 2022 LSC is visible a central empty region, due to the lack of data, mentioned previously.

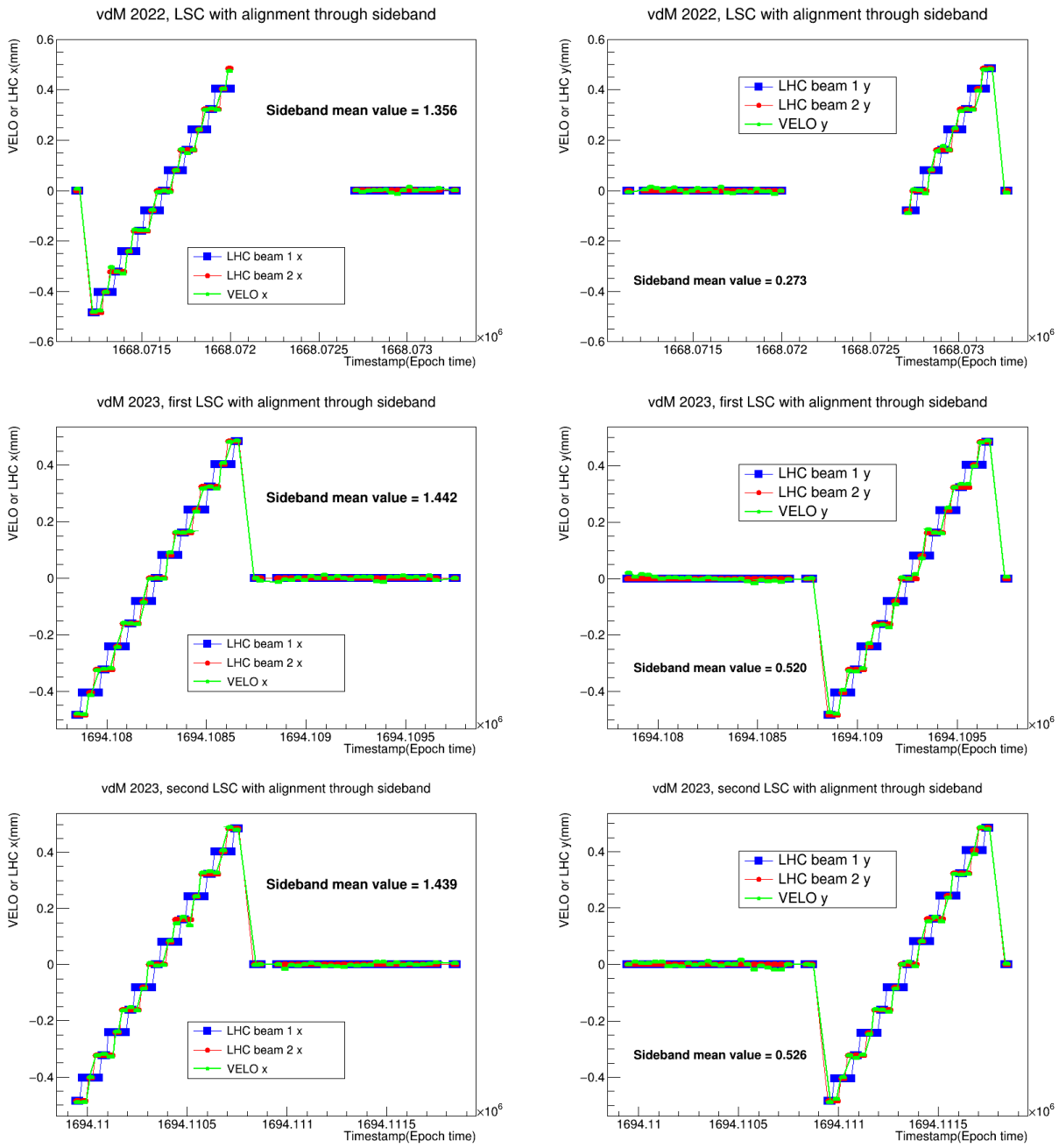

Figure 3.14: Beam 2 measured position and both beams nominal positions, aligned using the "sideband method", plotted against time steps. In the graphs showing the 2022 LSC is visible a central empty region, due to the lack of data, mentioned previously.

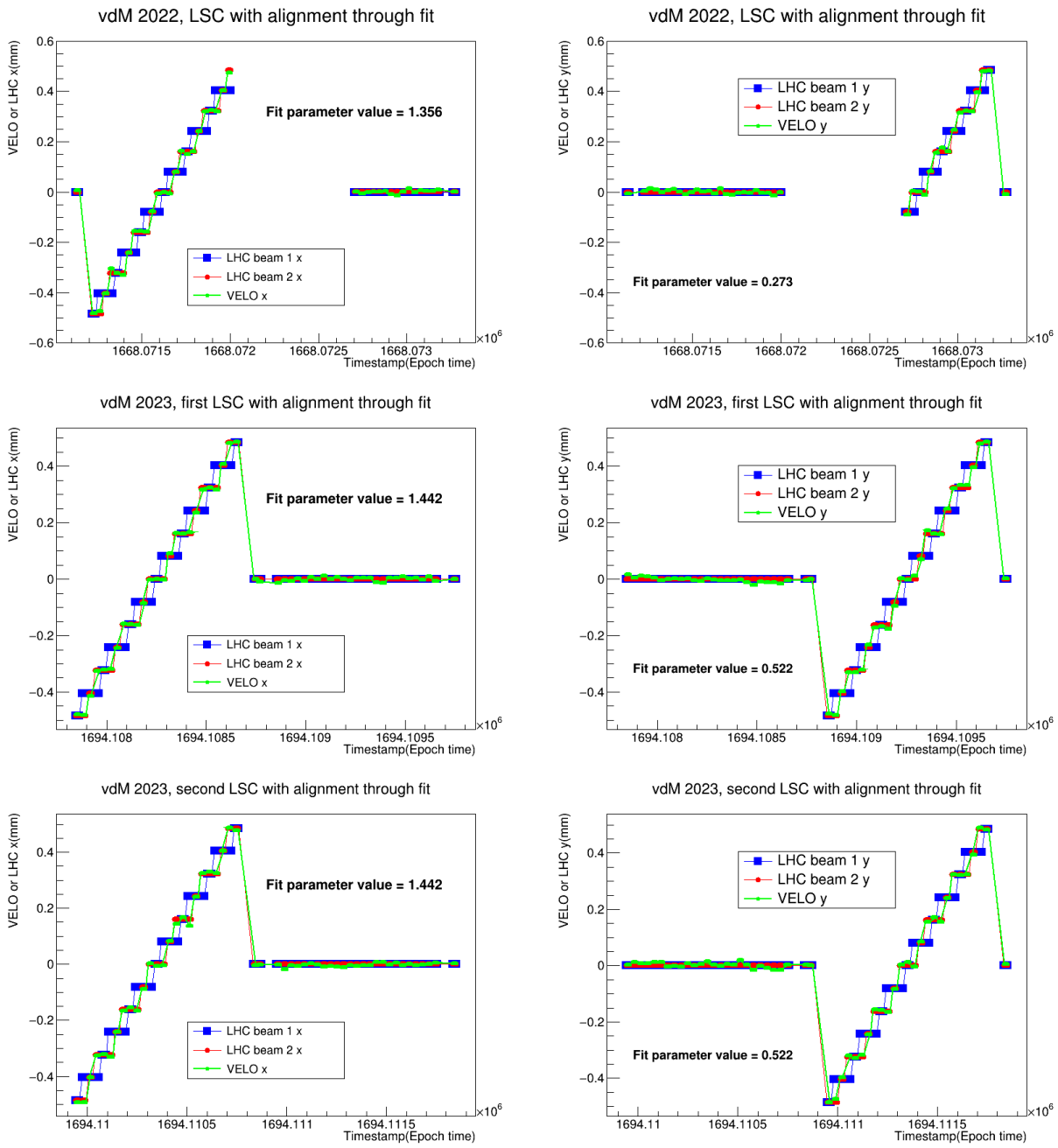

Figure 3.15: Beam 2 measured position along with both beam nominal positions, aligned using the "fit method", plotted against time steps. In the graphs showing the 2022 LSC is visible a central empty region, due to the lack of data, mentioned previously.

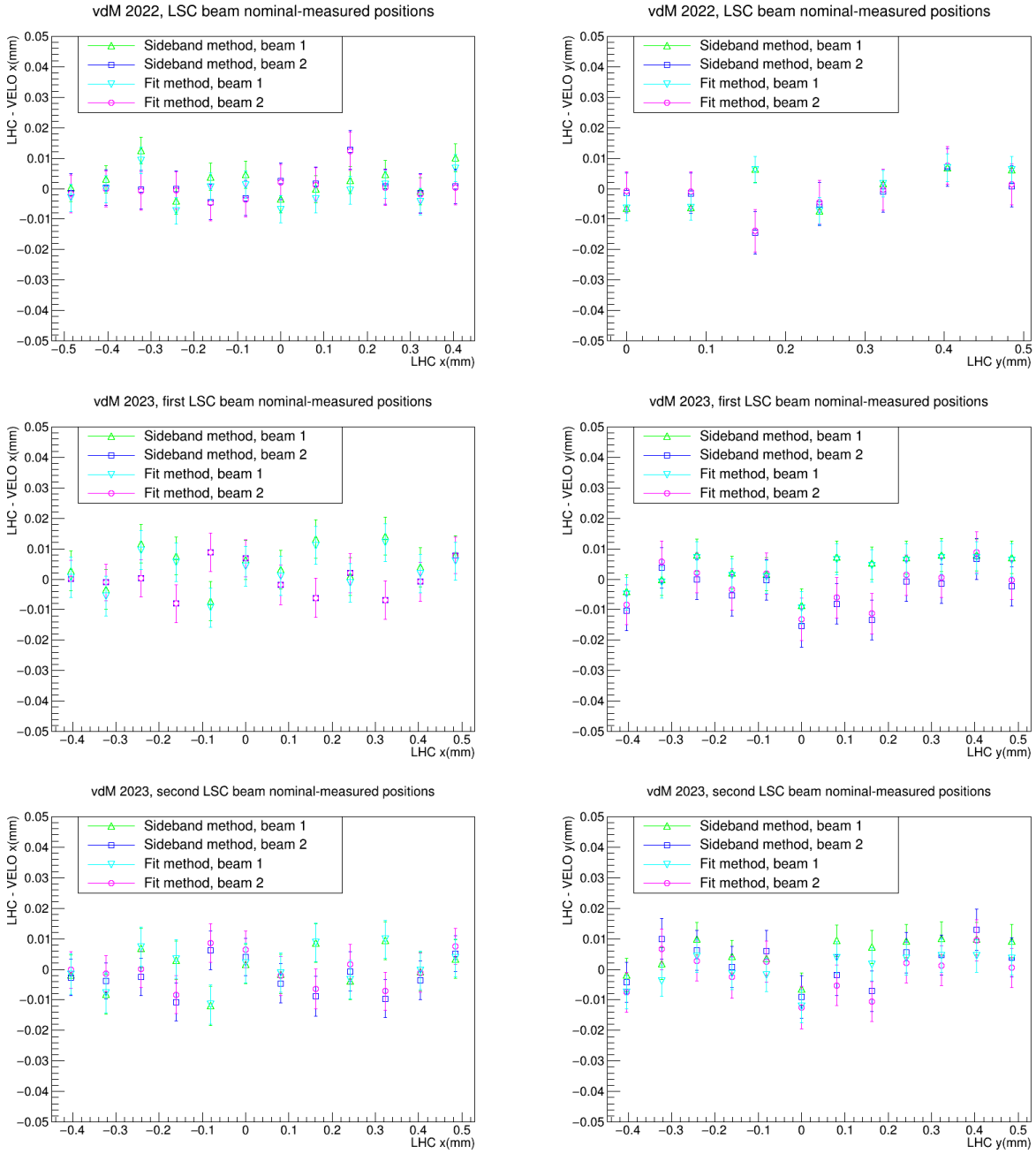

Figure 3.16: Difference of the beam nominal and measured positions, after applying the "sideband method"or the "fit method", plotted against the beam nominal position. In the graph showing the 2022 LSC along the y-axis there are fewer points than the others because of the lack of data mentioned previously.

3.3 Results

The mean values of the beam measured displacements derived from the constant beam separation method and the beam-gas imaging method are shown in Table 3.1 and 3.2, respectively. The nominal beam displacements for all the length scale calibration procedures analysed are as follows:

- $\Delta x_{LHC} = 0.0807$ mm; $\Delta y_{LHC} = 0.0807$ mm.

The uncertainty on the nominal beam displacements ($\sigma_{\Delta x, y_{LHC}}$) was assumed to be zero.

	$\Delta x_{VELO}(mm)$	$\Delta y_{VELO}(mm)$
LSC 2022	0.07956 ± 0.00004	0.08024 ± 0.00005
First LSC 2023	0.07751 ± 0.00012	0.07742 ± 0.00016
Second LSC 2023	0.07713 ± 0.00012	0.07751 ± 0.00015

Table 3.1: Mean values of the beam measured displacements obtained from the constant beam separation method.

	$\Delta x_{VELO}(mm)$	$\Delta y_{VELO}(mm)$
LSC 2022 beam 1	0.080 ± 0.002	0.079 ± 0.002
LSC 2022 beam 2	0.081 ± 0.003	0.082 ± 0.004
First LSC 2023 beam 1	0.081 ± 0.003	0.081 ± 0.002
First LSC 2023 beam 2	0.080 ± 0.003	0.080 ± 0.003
Second LSC 2023 beam 1	0.080 ± 0.003	0.080 ± 0.002
Second LSC 2023 beam 2	0.081 ± 0.003	0.081 ± 0.003

Table 3.2: Mean values of the beam measured displacements derived from the beam-gas imaging method.

The uncertainty on the mean value of each beam measured displacement was computed by adding quadratically the uncertainties on the beam measured displacements used to evaluate the mean value. In turn, the uncertainty on the single beam measured displacement was evaluated by adding quadratically the uncertainties on the beam measured positions. Finally, the uncertainties on the beam measured positions were taken directly from the vertex distributions, i.e., the uncertainties associated with the mean values of the histograms shown in Figures 3.3, 3.8 and 3.9.

The mean value of the length scale calibration constants was computed using the following formulas:

$$C_x = \frac{1}{N}\sum_{i=1}^{N}\frac{\Delta x_{VELO}(i)}{\Delta x_{LHC}} - 1; \tag{3.5}$$

$$C_y = \frac{1}{M}\sum_{i=1}^{M}\frac{\Delta y_{VELO}(i)}{\Delta y_{LHC}} - 1; \tag{3.6}$$

where N,M are the numbers of steps in which the sums are extended. The uncertainties of the constants were evaluated, adding quadratically the uncertainties of the terms in the sums. The uncertainty on each term of the sums was evaluated as follows:

$$\sigma_i = \frac{\sigma_{\Delta k_{VELO}(i)}}{\Delta k_{LHC}}, \tag{3.7}$$

where $k = x, y$ and $\sigma_{\Delta k_{VELO}(i)}$ is the uncertainty of the measured displacement "i".
The length scale calibration constants measured with the constant beam separation method are as follows:

- LSC 2022: $C_x = -0.0141 \pm 0.0005$; $C_y = -0.0057 \pm 0.0007$;
- First LSC 2023: $C_x = -0.0396 \pm 0.0015$; $C_y = -0.0407 \pm 0.0019$;
- Second LSC 2023: $C_x = -0.0442 \pm 0.0015$; $C_y = -0.0395 \pm 0.0019$.

The difference between the uncertainties of the constants in the 2022 and 2023 LSC is thought to be caused by several factors:

- Histograms' entries: the number of entries in the 2022 histograms, containing beam-beam vertices, was about 5 times greater than in the 2023 histograms.
- Histograms' width: the standard deviations of the 2022 histograms, containing beam-beam vertices, were about 20% smaller than those of the 2023 histograms.
- VELO's failure: during the 2023 vdM scan the VELO was not closed due to a mechanical failure, which did not occur in the 2022 scan.

The length scale calibration constants measured with the beam-gas imaging method are as follows:

- LSC 2022:
  - Beam 1: $C_x = -0.010 \pm 0.024$; $C_y = -0.020 \pm 0.029$;
  - Beam 2: $C_x = -0.002 \pm 0.032$; $C_y = \quad 0.013 \pm 0.044$;
- First LSC 2023:
  - Beam 1: $C_x = \quad 0.004 \pm 0.034$; $C_y = \quad 0.003 \pm 0.027$;
  - Beam 2: $C_x = -0.003 \pm 0.033$; $C_y = -0.004 \pm 0.033$;
- Second LSC 2023:
  - Beam 1: $C_x = -0.013 \pm 0.032$; $C_y = -0.014 \pm 0.027$;
  - Beam 2: $C_x = \quad 0.001 \pm 0.031$; $C_y = \quad 0.002 \pm 0.034$.

The uncertainties in the 2022 LSC constants are different for beam 1 and beam 2, while in 2023 they are not. This difference is thought to be due to the fact that in 2022, with the VELO closed, beam-empty events passed through many VELO stations, whereas empty-beam events passed through only a few. This could lead to a different vertex resolution and, consequently, a different uncertainty. The same reasoning does not apply to 2023 due to the previously mentioned mechanical failure of the VELO.
The results obtained using the beam-gas imaging method are compatible with zero and are consistent with the constant beam separation method within roughly one standard deviation. On the other hand, the constants obtained through the constant beam separation method show a 4% maximum difference with respect to the perfect displacements hypothesis. The discrepancy between the nominal and measured beam displacements is evident in Figure 3.7. The underlying cause of this phenomenon is not yet understood and will be investigated continuing the work started with this thesis.

Conclusions

Accurate knowledge of detector luminosity is crucial for precise measurements in high-energy physics experiments. A widely used method for calibrating luminosity at the LHC is the van der Meer scan, which involves controlled movements of the particle beams to determine the beam profiles. In each van der Meer scan the precision of these beam movements is verified through the length scale calibration procedure.
This thesis presents an analysis of the data from three length scale calibration procedures performed at the LHCb experiment, during two van der Meer scans conducted in 2022 and 2023. The accuracy of the beam movements was evaluated by measuring the length scale calibration constants, using two distinct methods: the constant beam separation method and the beam-gas imaging method. These methods require knowledge of both the nominal beam displacements, provided by the LHC, and the effective beam displacements, determined using interaction vertex data collected by the VELO detector. Specifically, the constant beam separation method relies on the reconstruction of the position of the interaction vertices created when two bunches collide, whereas the beam-gas imaging method exploits the interaction of single beams with the gas injected in the VELO vessel.
The length scale calibration constants measured with the constant beam separation method are as follows:

- LSC 2022: $C_x = -0.0141 \pm 0.0005$; $C_y = -0.0057 \pm 0.0007$;
- First LSC 2023: $C_x = -0.0396 \pm 0.0015$; $C_y = -0.0407 \pm 0.0019$;
- Second LSC 2023: $C_x = -0.0442 \pm 0.0015$; $C_y = -0.0395 \pm 0.0019$.

The length scale calibration constants measured with the beam-gas imaging method are as follows:

- LSC 2022:
  - Beam 1: $C_x = -0.010 \pm 0.024$; $C_y = -0.020 \pm 0.029$;
  - Beam 2: $C_x = -0.002 \pm 0.032$; $C_y = \quad 0.013 \pm 0.044$;

- First LSC 2023:
  - Beam 1: $C_x = \quad 0.004 \pm 0.034$; $C_y = \quad 0.003 \pm 0.027$;
  - Beam 2: $C_x = -0.003 \pm 0.033$; $C_y = -0.004 \pm 0.033$;
- Second LSC 2023:
  - Beam 1: $C_x = -0.013 \pm 0.032$; $C_y = -0.014 \pm 0.027$;
  - Beam 2: $C_x = \quad 0.001 \pm 0.031$; $C_y = \quad 0.002 \pm 0.034$.

The values obtained using the beam-gas imaging method are consistent with zero and are consistent within roughly one sigma with the measurements performed with the constant beam separation method. However, the results from the constant beam separation method show a 4% discrepancy with respect to the LHC declared beam positions. The reason for this discrepancy is not known yet and will be investigated by further studies based on the work described in this thesis.

Bibliography

[1] Vladislav Balagura. "Van der Meer scan luminosity measurement and beam–beam correction". In: *The European Physical Journal C* 81.26 (2021). DOI: 10.1140/epjc/s10052-021-08837-y. URL: https://doi.org/10.1140/epjc/s10052-021-08837-y.

[2] Werner Herr e Bruno Muratori. "Concept of luminosity". In: *CAS - CERN Accelerator School: Intermediate Accelerator Physics* (2006), P361–P378. DOI: 10.5170/CERN-2006-002.361. URL: https://cds.cern.ch/record/941318.

[3] LHCb Collaboration. *The LHCb Upgrade I*. Tech. rep. 2023. URL: https://doi.org/10.48550/arXiv.2305.10515.

[4] The LHCb collaboration. "Precision luminosity measurements at LHCb". In: *Journal of Instrumentation* 9.12 (Dec. 2014), P12005–P12005. DOI: 10.1088/1748-0221/9/12/p12005. URL: https://doi.org/10.1088/1748-0221/9/12/p12005.

[5] I. Belyaev G. Carboni N. Harnew C. Matteuzzi e F. Teubert. "The history of LHCb". In: *The European Physical Journal H* 46.3 (2021). DOI: 10.1140/epjh/s13129-021-00002-z. URL: https://doi.org/10.1140/epjh/s13129-021-00002-z.

[6] Ewa Lopienska. *The CERN accelerator complex, layout in 2022. Complexe des accélérateurs du CERN en janvier 2022*. General Photo. 2022. URL: https://cds.cern.ch/record/2800984.

[7] Lyndon Evans e Philip Bryant. "LHC Machine". In: *Journal of Instrumentation* 3 (Aug. 2008), S08001. DOI: 10.1088/1748-0221/3/08/S08001. URL: https:%20//dx.doi.org/10.1088/1748-0221/3/08/S08001.